

UNIVERSITY OF OKLAHOMA
GRADUATE COLLEGE

GLOBAL LARGE-SCALE STRATOSPHERE-TROPOSPHERE EXCHANGE
IN MODERN REANALYSES

A THESIS

SUBMITTED TO THE GRADUATE FACULTY

in partial fulfillment of the requirements for the

Degree of

MASTER OF SCIENCE IN METEOROLOGY

By

ALEXANDER C. BOOTHE
Norman, Oklahoma
2016

GLOBAL LARGE-SCALE STRATOSPHERE-TROPOSPHERE EXCHANGE
IN MODERN REANALYSES

A THESIS APPROVED FOR THE
SCHOOL OF METEOROLOGY

BY

Dr. Cameron R. Homeyer, Chair

Dr. Petra Klein

Dr. Alan Shapiro

© Copyright by ALEXANDER C. BOOTHE 2016
All Rights Reserved.

Acknowledgments

Most of all, I have to thank my mother, sisters, and loving girlfriend. They have believed in me from day one. Their belief and knowledge has helped guide me through the past, the present, and (I'm sure) will in the future. They have meant the world to me throughout this project and my life. Without them, I would have not made it this far nor be the person I am today.

My advisor and friend, Dr. Cameron Homeyer, gave me the opportunity to work with him as his first graduate student. Although there was confusion during my recruitment (the unread e-mail!), I am very glad he still offered me a position in his research group. I have learned so much about being a research scientist and have gained many tools for my 'tool box' as a researcher (from programming to making aesthetically pleasing figures). Not only did I learn invaluable researching skills as his student, I also benefited from his wisdom and knowledge about life over the past 2 years. I am truly grateful and honored that he gave me this once in a lifetime opportunity. Thank you.

I would also like to thank my committee members: Dr. Alan Shapiro and Dr. Petra Klein. Both of them have been helpful and willing to guide me throughout this project.

Furthermore, I would like to thank (the soon to be Dr.) Daniel Phoenix, Shawn Handler, and Thea Sandmæl. All three of them have helped me throughout this project, although they may have not realized it. From the lunch time powwows to the O'Connell shuffleboard table (and the push-ups in between), each of them

have always been willing to sit, listen, and engage themselves during research discussions and presentations. Thank you all for being apart of this project.

Others, outside of the University, have also been important to this project. I would like to thank Bojan Škerlak and Michael Sprenger for allowing us to use data from their early STE study to be compared to our analyses. Also, I would like to thank the agencies that provide reanalysis meteorological output used in this project and many others: ECMWF (ERA-Interim), JMA (JRA-55), and NASA (MERRA-1/2).

Finally, thanks to the University of Oklahoma for giving me the opportunity to study and build my meteorological knowledge in a place where the atmosphere reveals it's true beauty.

Table of Contents

| | |
|---|-------------|
| Acknowledgments | iv |
| List of Figures | viii |
| List of Tables | xi |
| Abstract | xii |
| 1 Introduction and Background | 1 |
| 1.1 Stratosphere-troposphere exchange | 1 |
| 1.2 Large-scale STE processes | 2 |
| 1.2.1 Extratropical STE processes | 2 |
| 1.2.2 Tropical STE processes | 3 |
| 1.2.3 Intermediate: subtropical STE processes | 3 |
| 1.3 Analyzing STE | 4 |
| 1.3.1 Eulerian-based STE | 4 |
| 1.3.2 Lagrangian-based STE | 5 |
| 1.4 STE challenges | 6 |
| 2 Data and methods | 8 |
| 2.1 Reanalysis model output | 8 |
| 2.2 Tropopause definition | 9 |

| | | |
|----------|---|-----------|
| 2.3 | STE identification | 10 |
| 2.4 | Categorizing STE | 12 |
| 3 | STE method comparison | 14 |
| 4 | Results | 16 |
| 4.1 | STE geographic distribution | 16 |
| 4.2 | STE totals | 19 |
| 4.3 | STE meridional distributions | 20 |
| 4.4 | Annual cycles | 21 |
| 4.5 | STE time series | 23 |
| 4.6 | Reanalysis model evaluations | 25 |
| 4.6.1 | STE occurrence geographic distributions | 26 |
| 4.6.2 | Diagnostics | 26 |
| 5 | Conclusions and discussion | 29 |
| 5.1 | Principal conclusions | 29 |
| 5.2 | Discussion | 32 |
| | Bibliography | 34 |
| | Appendix A | |
| | Figures & Tables | 39 |

List of Figures

| | | |
|---|---|----|
| 1 | Schematic of STE identification method. Vertical STT and TST are shown by orange and blue arrows, respectively. Bold and wavy arrows represent Brewer–Dobson circulation and quasi-isentropic mixing processes, respectively. Potential temperature surfaces are given by the cyan lines, the lapse-rate tropopause by the black lines, and the 2 pvu PV isosurface by the green line. The solid gray line, coincident with the tropopause break (dashed black line), represents the boundary between the tropics and extratropics. Subtropical and polar jet streams are shown by solid purple isotachs. | 40 |
| 2 | December, January, and February (DJF, top row) and June, July, and August (JJA, bottom row) mean STT mass fluxes for 1996–2010 using the lapse-rate tropopause method (left) and 1979–2011 using the dynamic tropopause method (right; from Škerlak et al. (2014)). | 41 |
| 3 | As in Fig. 2, but for TST. | 42 |
| 4 | Annual mean geographic distributions of total STE mass flux for ERA-Interim (a & b), JRA-55 (c & d), MERRA-2 (e & f), and MERRA-1 (g & h). STE is separated into STT (left) and TST (right) for each reanalysis. | 43 |
| 5 | As in Fig. 4, but for vertical STE in the extratropics. | 44 |
| 6 | As in Fig. 4, but for the vertical STE in the tropics. | 45 |

| | | |
|----|---|----|
| 7 | As in Fig. 4, but for lateral STE. | 46 |
| 8 | Annually and zonally averaged meridional distributions of STE from each reanalysis function of latitude and for (a) total STE, (b) vertical STE, and (c) lateral STE. STT is shown as the dotted lines (negative), TST as the dashed lines (positive), and the net transport is given by the solid lines in each panel. STE from JRA-55 is shown by the purple lines, ERA-Interim by the blue lines, and MERRA-2 and MERRA-1 by the light and dark red lines, respectively. | 48 |
| 9 | Annual cycles of (top row) normalized STT and (bottom row) normalized TST for the (left) Northern Hemisphere and (right) Southern Hemisphere from each reanalysis model. In each plot, the solid colored lines are the mean annual cycles and the colored error bars are plus/minus one standard deviation from the mean. STE from JRA-55 is shown by the purple lines, ERA-Interim by the blue lines, and MERRA-2 and MERRA-1 by the light and dark red lines, respectively. Note that SH and NH annual cycles are offset by 6 mo. | 49 |
| 10 | As in Figure 9, but for non-normalized net total STE (top row), net vertical STE (middle row), and net lateral STE (bottom row). | 51 |
| 11 | For each reanalysis, time series of globally integrated (top) total, (bottom) lateral, and (middle) vertical STT (left) and TST (right) mass fluxes that are normalized by the 15-year mean over the period (1996–2010). The thin lines represent the monthly mean mass fluxes, while the bold lines are the result of applying a low-pass filter to a Fourier transform of each time series (power at time scales \leq 12 months is attenuated). STE from JRA-55 is shown by the purple lines, ERA-Interim by the blue lines, and MERRA-2 and MERRA-1 by the light and dark red lines, respectively. | 52 |

| | | |
|----|--|----|
| 12 | As in Fig. 11, but for vertical STE in the (top) tropics and (bottom) extratropics. | 53 |
| 13 | Global occurrence frequency distributions of (left) STT and (right) TST events for (a & b) ERA-Interim, (c & d) JRA-55, (e & f) MERRA-2, and (g & h) MERRA-1. | 54 |
| 14 | Monthly (November 2002) tropopause break-relative zonal means of (a) tropopause pressure (hPa) and (b) total horizontal wind (m s^{-1}) for each reanalysis. JRA-55 is shown by the purple lines, ERA-Interim by the blue lines, and MERRA-2 and MERRA-1 by the light and dark red lines, respectively. | 55 |
| 15 | Geographic distributions of TST mass flux (top row) and occurrence (bottom row) using JRA-55 reanalysis diabatic (left; K s^{-1}) and kinematic (right; hPa s^{-1}) vertical velocity output over the 15-year period (1996–2010). | 56 |

List of Tables

- A.1 Globally integrated STE mass fluxes averaged over the 15-yr period for each reanalysis model. STT, TST, net (TST-STT), and gross (TST+STT) mass fluxes are given for each transport category (i.e. total, vertical, and lateral exchange). All mass flux units are 10^{10} kg s^{-1} 47
- A.2 STT and TST annual cycle amplitudes given in both hemispheres from each reanalysis model. All amplitudes are in units of 10^9 kg s^{-1} . 50

Abstract

Stratosphere-troposphere exchange (STE) has important and significant impacts on the chemical and radiative properties of the upper troposphere and lower stratosphere. This study presents a 15-year climatology of global large-scale STE from four modern reanalyses: ERA-Interim, JRA-55, MERRA-2, and MERRA-1. STE is separated into four categories for analysis to identify the significance of known transport mechanisms: 1) vertical stratosphere-to-troposphere transport (STT), 2) vertical troposphere-to-stratosphere transport (TST), 3) lateral STT (that occurring between the tropics and the extratropics and across the tropopause “break”), and 4) lateral TST.

In addition, this study employs a method to identify STE as that crossing the lapse-rate tropopause (LRT), while most previous studies have used a potential vorticity (PV) isosurface as the troposphere-stratosphere boundary. PV-based and LRT-based STE climatologies are compared using the same reanalysis output (ERA-Interim). The comparison reveals quantitative and qualitative differences, particularly in the geographic representation of TST in the polar regions.

Based upon spatiotemporal integrations among the reanalysis models, we find STE to be STT-dominant in ERA-Interim and JRA-55 and TST-dominant in the MERRA reanalyses. Time series analysis over the 15-year period show long-term changes in STT and TST, which are argued to correspond with changes in the Brewer-Dobson circulation. Ultimately, differences occur as a result of physical and dynamical differences between the four reanalysis models.

Chapter 1

Introduction and Background

1.1 Stratosphere-troposphere exchange

Stratosphere-troposphere exchange (STE) has important and significant impacts on the chemical and radiative properties of the upper troposphere and lower stratosphere (UTLS). Oxidative and greenhouse gases can be transported across the tropopause in two directions, typically referred to as stratosphere-to-troposphere transport (STT) and troposphere-to-stratosphere transport (TST) (Holton et al., 1995). STT brings ozone-rich stratospheric air into the troposphere, and in some cases STT can extend into the planetary boundary layer (Danielsen, 1968; Lin et al., 2012). Per molecule, ozone radiative forcing is maximized in the upper troposphere (Lacis et al., 1990). Conversely, TST processes can inject water vapor and other tropospheric pollutants into the lower stratosphere, where the lifetimes of such gases can be increased. Because water vapor is a greenhouse gas, increases in LS water vapor from TST lead to an increase in radiative forcing similar to that for UT ozone (Forster and Shine, 2002).

1.2 Large-scale STE processes

STE is driven by dynamic processes occurring across a wide range of spatial and temporal scales. There are several known large-scale processes that occur in the extratropical domain, the tropical domain, and along the boundary between them (i.e. within the subtropics).

1.2.1 Extratropical STE processes

STE in the extratropics often occurs in the vicinity of baroclinic transient eddies, or extratropical cyclones (Holton et al., 1995; Wernli and Davies, 1997; Wirth and Egger, 1999; Reutter et al., 2015). Transport associated with extratropical cyclones is dominated by STT, and is primarily due to clear-air turbulence along the edges of stratospheric intrusions (or tropopause folds) in the upper-troposphere (Danielsen, 1968; Shapiro, 1980; Lamarque and Hess, 1994; Cooper et al., 2004; Reutter et al., 2015). Stratospheric intrusions can develop apart from extratropical cyclones along the cyclonic side of upper tropospheric jet streams as a result of ageostrophic circulations (Sawyer, 1956; Shapiro, 1981; Shapiro and Kennedy, 1981; Keyser and Shapiro, 1986). These tend to be shallow and exchange less than stratospheric intrusions associated with extratropical cyclones (Wernli and Bourqui, 2002; Sprenger and Wernli, 2003). Extratropical cyclones also result in TST, which is sourced by warm-conveyor-belt flows that bring lower troposphere air to the UTLS along isentropic surfaces and by moist convection. (Stohl, 2001; Wernli and Bourqui, 2002; Reutter et al., 2015). Cut-off extratropical cyclones occur frequently in the upper-troposphere and result in STT due to eroding processes (i.e. turbulence and friction) acting on the associated depression in the tropopause (Price and Vaughan, 1993).

1.2.2 Tropical STE processes

STE has been found to be globally unbalanced, with net TST in the tropics and net STT in the extratropics. This imbalance is primarily a reflection of systematic tropospheric upwelling at the tropical tropopause and downwelling at the extratropical tropopause that is driven by the diabatic Hadley cell and Brewer-Dobson circulation (or BDC) (Brewer, 1949; Dobson, 1956). The BDC is roughly a 2-year latitudinal circulation, where tropospheric air diabatically ascends into the tropical lower-stratosphere and is dynamically “pumped” poleward and downward into the extratropical lower stratosphere by Rossby wave breaking in the mid-latitudes (Holton et al., 1995). Apart from the BDC, TST in monsoon anticyclones is an important STE mechanism in the tropics. Moist convection rapidly lofts lower troposphere air into the interior of the UT anticyclonic circulation where it slowly ascends into the lower stratosphere. The North American and Asian Monsoon Anticyclones are receiving a considerable amount of recent attention and have been shown to contribute significantly to global STE (e.g. Randel et al., 2010, and references therein).

1.2.3 Intermediate: subtropical STE processes

There are also known STE processes that occur primarily in the subtropics and involve tropical UT air and extratropical LS air. One of the most well-known subtropical STE processes is Rossby wave breaking, which is a quasi-isentropic transport process that can be predominantly poleward (TST), equatorward (STT), or bidirectional (Seo and Bowman, 2001; Scott and Cammas, 2002; Homeyer and Bowman, 2013). Stratospheric intrusions along the subtropical jet stream occur outside of the tropics, but can bring extratropical lower stratosphere air into the

tropical middle and upper troposphere (Waugh and Polvani, 2000).

1.3 Analyzing STE

1.3.1 Eulerian-based STE

The impacts of STE are considerable on the global scale but, as a result of limited observations, most studies have investigated STE and associated large-scale processes over small domains and for short time periods using numerical models and remote sensing or aircraft platforms. For example, Lamarque and Hess (1994) used a simulated stratospheric intrusion to estimate the annual net mass exchange across the tropopause in the Northern Hemisphere by extrapolation. Specifically, annual estimates of STT were approximated using an annual average of stratospheric intrusions (1460 per year) and STT quantities found in their case study, which amounted to 1.79×10^{17} kg per year. Although quantitative estimates from Lamarque and Hess (1994) were similar to additional studies published at the time, they suggested that stratospheric intrusions are invariable and exhibit similar lifespans and STE quantities, which is now known to be an incorrect assumption. Modern numerical models and computing capabilities, however, enable climatological studies of STE without estimation or extrapolation using a limited number of events.

Previous studies have employed multiple years of global model output to produce a climatology of STE. Appenzeller et al. (1996) analyzed downward fluxes out of the lower stratosphere in the Northern and Southern Hemispheres over two calendar years (1992 and 1993). The study emphasized an Eulerian approach, the “downward control principle” (i.e. mass continuity), to estimate seasonal net flux in the extratropics, and results indicated a peak downward flux during Northern

Hemisphere spring. Annual net downward mass flux was estimated to be 3.5×10^{17} kg and 3.3×10^{17} kg for the Northern and Southern hemispheres, respectively, which is nearly twice that found by Lamarque and Hess (1994). An important caveat in the Appenzeller et al. (1996) study is that the method does not provide spatial distributions of STE and only considers STT in the extratropics. Another Eulerian metric used as a diagnostic for STE is the Wei method (Wei, 1987), which allows for determination of STT and TST on short spatiotemporal scales but suffers from conceptual problems (Gettelman and Sobel, 2000).

1.3.2 Lagrangian-based STE

An alternative to Eulerian methods is a Lagrangian approach, which employs a large number of three-dimensional (or 3-D) trajectories to determine STE. For example, Stohl (2001) developed a one-year Northern Hemisphere climatology of STE using trajectories and identified large-scale airstreams and the corresponding spatial and temporal variability of STE associated with particular flows (i.e. warm-conveyor belts and stratospheric intrusions). Annual net downward mass flux estimates in the northern extratropics were found to be larger than previous global estimates (4.4×10^{17} kg).

Multi-year climatologies of STE have also employed a Lagrangian approach on global and hemispherical scales, wherein studies aim to investigate the quantitative and qualitative characteristics of STE (Wernli and Bourqui, 2002; Sprenger and Wernli, 2003; Škerlak et al., 2014). A recent STE climatology by Škerlak et al. (2014, hereafter Š14) evaluated STE over a 33-year period using 3-D kinematic winds from the ERA-Interim reanalysis and a Lagrangian trajectory model. Their method requires a parcel to remain in its parent reservoir (troposphere or stratosphere) and destination reservoir (stratosphere or troposphere) for at least 48

hours to be classified as irreversible STE (a so-called ‘residence time’). Although a Lagrangian trajectory method was employed, the annual downward net exchange found (0.42×10^{17} kg yr⁻¹) was an order of magnitude smaller than estimates by Stohl (2001). It is apparent that residence times significantly decrease the quantitative STE estimates as a result of separating irreversible exchange from transient exchange.

1.4 STE challenges

As outlined above, there have been three classes of methods used to analyze STE: (1) Eulerian based approaches, such as the Wei method and the “downward control principle”, (2) a Lagrangian trajectory-based method that does not use a residence filter (e.g. Stohl, 2001; Seo and Bowman, 2002), and (3) a Lagrangian trajectory-based method with a residence filter (e.g. Wernli and Bourqui, 2002; Sprenger and Wernli, 2003; Škerlak et al., 2014). Despite previous efforts to determine climatological characteristics of STE, the various models, methods, and time periods used have led to a wide range of transport estimates.

Motivated by an improved understanding of UTLS characteristics and processes and the availability of output from numerous higher resolution global models, this study seeks to develop and contrast climatological estimates of STE from several modern global reanalyses: the European Centre for Medium-range Weather Forecasting Interim reanalysis (ERA-Interim), the Japanese Meteorological Agency 55-year reanalysis (JRA-55), and the National Aeronautics and Space Administration (NASA) Modern Era Retrospective analysis for Research and Applications versions 1 and 2 (MERRA-1/2). A Lagrangian approach is applied using 3-D kinematic wind fields from each reanalysis to compute STE during a 15-year period: 1996-2010. STE is further stratified into four categories in an attempt to

evaluate the role of individual large-scale transport processes on the global scale: vertical STT, vertical TST, lateral (quasi-horizontal) STT, and lateral TST. While small-scale mechanisms such as gravity wave breaking and convection contribute to STE as well, such processes are not investigated in this study because they are not resolved in the reanalyses.

Chapter 2

Data and methods

2.1 Reanalysis model output

As outlined in Section 1, we employ output from four reanalysis models in this study: ERA-Interim, JRA-55, MERRA-1, and MERRA-2. ERA-Interim is available from 1979–present on an approximately 80 km horizontal grid and at 60 vertical model levels with a model top of 0.1 hPa (Dee et al., 2011). JRA-55 is available from 1958–present on a ~ 60 km horizontal grid (Kobayashi et al., 2015). Similar to ERA-Interim, JRA-55 has 60 vertical model levels with a model top of 0.1 hPa. MERRA-1 is available from 1979–2016 at $0.5^\circ \times 0.667^\circ$ horizontal resolution and at 72 vertical model levels with a model top of 0.01 hPa (Rienecker et al., 2011). MERRA-2 has a similar design to MERRA-1, but is available at a slightly finer horizontal resolution of $0.5^\circ \times 0.625^\circ$ from 1979–present (Bosilovich et al., 2015). Numerical improvements from MERRA-1 to MERRA-2 are expected to more accurately resolve UTLS processes. Comparison of their STE representations will demonstrate model improvements.

We employ 3-D output at 6-hour intervals from each reanalysis in this study. All of the data is interpolated to a regular $1^\circ \times 1^\circ$ latitude-longitude grid for analysis. Model output is also used to calculate secondary variables for analysis: tropopause pressure (using the World Meteorological Organization (WMO) (1957)

lapse-rate tropopause (LRT) definition), potential temperature (θ), and potential vorticity (PV) on the native model levels.

2.2 Tropopause definition

The tropopause definition employed in STE studies is critical to their outcome since it represents the boundary between troposphere and stratosphere and the location where dynamical processes and associated transport are evaluated. Many previous STE studies have used a “dynamical” tropopause to represent the troposphere-stratosphere boundary, for which a potential vorticity (PV) isosurface such as 2-PVU ($1 \text{ PVU} = 10^{-6} \text{ Km}^2\text{kg}^{-1}\text{s}^{-1}$) is used (Ertel and Rossby, 1949). However, several studies demonstrate that STE estimates can be largely sensitive to small changes in the PV isosurface used. For example, Seo and Bowman (2002) (their Fig. 6) made Lagrangian estimates of STE using multiple control surfaces, including isobaric surfaces and potential vorticity iso-surfaces, and found downward mass flux ranged from $1\text{--}4 \times 10^{17} \text{ kg/yr}$. Homeyer and Bowman (2013) used 30 yr of ERA-Interim to produce a climatology of Rossby wave breaking events and associated STE in the subtropics and demonstrated that varying the PV boundary from 2 to 4 PVU resulted in a reversal of the net transport direction (i.e., TST or STT). Despite these known sensitivities, many studies have continued to employ a dynamic tropopause to avoid challenging STE calculations in the vicinity of the sharp LRT discontinuity near the subtropical jet known as the “tropopause break” (Palmén, 1948; Randel et al., 2007; Homeyer and Bowman, 2013). Because PV is a quasi-conserved quantity in an adiabatic and frictionless flow, it is treated as a quasi-material surface, and can provide a continuous boundary through the tropopause break. An additional aspect of a PV-based method that is problematic

for global STE studies is the fact that PV values converge to zero at the equator and do not coincide with the altitude of the tropical tropopause south of the tropopause break. As a result, most studies that use a PV-based method in the extratropics select an alternative surface to represent the tropopause in the tropics (e.g., cold point altitude, isentropic surface).

The LRT, on the other hand, has been shown to coincide best with stability and chemical transitions between the troposphere and stratosphere globally (e.g., Gettelman et al., 2011; Pan et al., 2004). This is due to the fact that a single PV value does not coincide with the LRT and chemical transition everywhere, with PV values at the tropopause ranging from at least 1 to 6 pvu in the extratropics (e.g., Kunz et al., 2011). For these reasons, we use the LRT to represent the troposphere-stratosphere boundary in this study, but leverage beneficial information from PV analyses to identify irreversible transport. A detailed outline of this approach is provided in the following subsection.

2.3 STE identification

Trajectory calculations (~ 6 billion) in this study are performed using the TRAJ3D model developed by Bowman (1993) and updated in Bowman and Carrie (2002). Parcels are initialized daily at 00 UTC every 1° in longitude and latitude and every 20 hPa at altitudes relative to the LRT. Analogous to STE methods in previous studies, preliminary selection of STE parcels is dependent upon whether trajectories cross the LRT within the initial 24 hours downstream. This selection is a straightforward process and only requires the initial and final parcel pressure and coincident tropopause pressure. For instance, if a parcel pressure is initially lower than its coincident tropopause pressure and one day downstream the parcel pressure is greater than its coincident tropopause pressure, it is flagged as possible

STT. All potential STE parcels are then advected 5 days forward and backward in time from the initial parcel locations for further analysis.

To ensure that transient (intermittent tropopause crossing) STE parcels are not erroneously counted and represented as irreversible exchange, a filtering method is applied to each parcel. Two criteria are necessary to identify irreversible transport: (i) a residence time (τ), and (ii) a parcel PV change occurring during the 10-day trajectory period. Based on a sensitivity study by Wernli and Bourqui (2002), a long residence time, longer than 24 hours, can decrease estimates of irreversible transport and change the direction of the annual net STE. Here, we chose a strict residence time criteria, τ , of 96 hours. This allows processes with longer transport times to be identified as STE, such as the slower diabatic upwelling in the tropics. The second filtering criteria requires an absolute PV change of 0.5 PVU from the initial parcel value to that 5 days downstream. The PV criteria represents a dynamic change in a parcel’s characteristics from the influence of diabatic or frictional affects (i.e., mixing). Parcels that meet the required criteria are retained as irreversible exchange.

To examine irreversible STE mass flux, we compute the mass of each parcel based on the following equation:

$$M = \frac{1}{g}(a_0^2 \cos \phi)\Delta\lambda\Delta\phi\Delta p \quad (2.1)$$

Where Earth’s gravitational acceleration and radius are denoted by g and a_0 , respectively, and ϕ , λ , and p represent latitude, longitude, and pressure scales of each parcel. Since the parcel resolution is constant, parcel mass decreases from equator to pole. Therefore, a greater number of transported parcels are required in the extratropical and polar latitudes to achieve equivalent STE to that in the tropics and subtropics. We bin STE parcels on a global grid with a longitude–latitude resolution of 2 degrees. For this purpose, the 1-day downstream parcel locations are used in an attempt to better represent the locations where STE occurred. Slight

differences in the locations of STE in the comparisons with Š14 in Chapter 3 may be due to this choice, since Š14 use their initial parcel locations for binning.

2.4 Categorizing STE

In an attempt to evaluate the role of individual large-scale STE processes globally, we separate transport into four categories: vertical STT, vertical TST, lateral STT, and lateral TST. For large-scale STE processes, lateral exchanges are known to correspond primarily with Rossby wave breaking. Vertical exchanges, however, are associated with extratropical cyclones, stratospheric intrusions, and tropical upwelling. Therefore, in addition to the four categories, we also separate vertical exchanges by geographic reservoir: tropical or extratropical. In particular, we classify regions as tropical if they lie equatorward of the ‘tropopause break’ and extratropical if they lie poleward of the break. Similar to previous studies, the tropopause break is defined as the LRT altitude frequency minimum between tropical (15-17 km or < 150 hPa) and extratropical (8-12 km or > 150 hPa) modes in hemispheric distributions (e.g., Birner, 2010; Homeyer and Bowman, 2013). Analysis of tropopause altitudes in each reanalysis model reveal that, despite slight differences in LRT altitudes, the tropopause break can be routinely identified in each using a tropopause pressure threshold of 150 hPa (not shown). Therefore, we set trajectories with vertical STE as tropical if the tropopause pressure at the initial parcel location is less than 150 hPa, and extratropical otherwise.

Similarly, classifying parcel transport as lateral or vertical involves evaluating both its tropopause break-relative location and tropopause-relative altitude during advection. In particular, if a parcel is initially located below the tropical tropopause and located above the extratropical tropopause 5 days downstream, it will be flagged as lateral TST. Alternatively, if a parcel is initially located above

the extratropical tropopause and below the tropical tropopause 5 days downstream, it is flagged as lateral STT. Remaining parcels are flagged as vertical exchange. There is one important exception that must be accounted for: stratospheric intrusions below the subtropical jet. In order to identify these parcels as vertical exchange, we require an additional condition for lateral STT: both initial and final parcel pressures must be less than (above) the initial extratropical tropopause pressure. For a detailed schematic of the identification method see Fig. 1.

Chapter 3

STE method comparison

As previously mentioned, there can be significant variability in climatological STE estimates based on the tropopause definition chosen to analyze exchange. Here, we use our STE geographic distributions from ERA-Interim to briefly illustrate some of the differences and similarities between our approach (i.e., using the LRT) and the recent STE climatology presented by Š14 that employs a dynamic tropopause (i.e. a PVU-isosurface of ± 2 -PVU) in the extratropics and the 380 K isentrope in the tropics. In Figure 2, the global summertime and wintertime geographic distributions of STT are shown for each approach. During both seasons, the locations of STT maxima and minima are largely similar between the methods, but the magnitude of STT mass flux is significantly larger using the PV-based tropopause definition, particularly in the extratropics.

On the other hand, TST geographic distributions (Fig. 3) are shown to be quantitatively and qualitatively different. Similar to the STT comparisons, PV-based TST is larger than that found with the LRT method in most places. However, there is a unique latitudinal dependence of the differences, with the largest differences found in the polar regions. For the LRT method, global TST maxima are found within the tropics (i.e. Monsoon anticyclones and systematic tropical upwelling), while TST in the extratropics and especially the polar regions is found to be comparatively weak. The opposite relationship is found using a dynamic

tropopause. According to our knowledge of large-scale processes associated with TST, the geographic distributions from the LRT-based climatology (Left column Fig. 3) agree more closely with known transport mechanisms.

The differences between the two methods may be rooted in the altitude placement of the tropopause definition used. The ± 2 -PVU surface (dynamic tropopause used in Š14), while at times may reside at similar altitudes compared to the LRT, often resides at lower altitudes with respect to the LRT (Pan et al., 2004; Gettelman et al., 2011; Kunz et al., 2011). Therefore, UT stirring or mixing may lead to erroneously flagged STT or TST parcels when using the dynamic tropopause.

Chapter 4

Results

Throughout the following chapter comparisons of STE among the four reanalysis systems are shown using various metrics. Here, we seek to reveal important similarities and differences in STE and the associated sub-categories of exchange between the reanalyses.

4.1 STE geographic distribution

Global spatial distributions of annually averaged STT and TST mass fluxes are shown in the right and left columns of Fig. 4, respectively. All of the models are similar regarding peak STT regions, with the largest differences found in contrasting the magnitudes of downward transport. Total STT mass fluxes are maximized along the Northern Hemisphere (NH) Atlantic and Pacific extratropical storm tracks in each reanalysis model. Among the four reanalyses, ERA-Interim and JRA-55 STT mass fluxes are largest (Fig. 4a and 4c) with a maximum of ~ 300 $\text{kg s}^{-1} \text{ km}^{-2}$ in the core of NH cyclone tracks. In the Southern Hemisphere (SH) the STT mass fluxes are largest within the subtropical latitudes along the western coasts of the continents. The largest SH STT maximum in each reanalysis is located along the subtropical coast of Chile. This is a confined but dominant region

of STT mass flux, and is greatest in JRA-55 ($\sim 350 \text{ kg s}^{-1} \text{ km}^{-2}$) and weakest in MERRA-1 ($\sim 200 \text{ kg s}^{-1} \text{ km}^{-2}$). Another common region of elevated STT in the SH occurs over a broad area in the extratropics along the west coast of Antarctica. A noteworthy difference among reanalyses regarding STT mass fluxes is found within the tropics, where the location of peak STT mass flux varies considerably. Peak regions of tropical STT are found along the equator across the Indian ocean in JRA-55 and ERA-Interim, but are found to be displaced south of the equator in both MERRA reanalyses.

Annually averaged geographic distributions of TST mass fluxes show considerably larger magnitudes and broader maxima within the tropical latitudes (right column Fig. 4) in all of the reanalyses compared to STT. Spatially, maxima in tropical TST mass fluxes coincide with minima in STT mass flux. Distinct maxima of tropical TST mass fluxes are evident in the South China Sea, the East Pacific, the Caribbean Sea, and Southeast Asia. Within the subtropics a narrow band of TST extends from China into the east Pacific and is consistent among the reanalyses. Comparison of TST among the reanalyses reveals two modes: regionally (or latitudinally) symmetric in ERA-Interim and JRA-55, and regionally asymmetric in the MERRA reanalyses. The regional asymmetry in the MERRA reanalyses is due to significantly enhanced TST mass fluxes in the extratropics compared to the remaining reanalyses, with extratropical TST near $\sim 400 \text{ kg s}^{-1} \text{ km}^{-2}$ globally in MERRA-1/2 and near $\sim 200 \text{ kg s}^{-1} \text{ km}^{-2}$ in ERA-Interim and JRA-55. Another inconsistency among the reanalyses is the location of peak TST in the tropical western Pacific. The peak tropical TST location in JRA-55 and ERA-Interim is highest in the NH but extends across the equator, whereas MERRA-1/2 show a peak located mostly in the NH.

To better understand the differences and similarities of STT and TST geographic distributions, we can decompose both transport directions into the vertical and lateral subcategories of exchange to determine their contributions to the differences observed in total (lateral + vertical) STE. The extratropical spatial distributions of vertical STT and TST are shown in Fig. 5. One significant characteristic shown is the dominance of vertical STT over vertical TST in the extratropics indicated by ERA-Interim, JRA-55, and MERRA-2, especially over the NH and SH storm tracks. MERRA-1, however, shows the opposite behavior.

As in the global STT distributions, the largest vertical STT mass fluxes in the extratropics coincide with the NH cyclone tracks. In the SH, the vertical STT mass fluxes are largest poleward of 60 deg S. Also, vertical STT maxima across the subtropical SH, particularly the Chilean coast, are detected but magnitudes are weaker than those in total STT. More generally, Vertical STT mass fluxes in the extratropics are largest in JRA-55 and weakest in MERRA-1.

Vertical TST in the extratropics, similar to STT, is found to be spatially consistent amongst the reanalyses, with the only apparent differences being the localized maxima near 60 deg N in MERRA-1/2 that are not observed in ERA-Interim or JRA-55. In addition, vertical TST in the extratropics in MERRA-1 is generally larger than the remaining reanalyses.

Vertical STT and TST mass fluxes and their geographic distributions within the tropics are shown in Fig. 6. While both TST and STT mass fluxes are similar in magnitude between the reanalyses, there are slight offsets in the location and width of the identified maxima. For example, no two models agree on the precise location, zonal extent, or meridional extent of the TST maxima in the western Pacific. The offsets in STT and TST maxima outlined in the discussion of Figure 4 above are also evident in the maps of vertical STT in the tropics.

Lastly, Figure 7 shows geographic distributions of lateral STT and TST from the four reanalyses. These maps reveal that lateral transport is 1) generally weaker than vertical transport in each model, 2) is dominated by poleward transport in each hemisphere (i.e. TST), and 3) is preferentially distributed over the ocean basins and extends poleward downstream of the ocean basins (in agreement with known evolution of Rossby wave breaking events, e.g., see Figure 9 of (Homeyer and Bowman, 2013)). In reference to the total STE geographic distributions, it is evident that the influence of poleward and equatorward lateral transport directly corresponds the subtropical maxima in STT and TST, which is expected due to its association with the tropopause break.

4.2 STE totals

In an effort to quantitatively summarize some of the apparent differences identified in the analysis of geographic distributions, globally integrated and annually averaged STE mass fluxes are provided in Table A.1 for each of the four reanalysis models. Total STT mass flux is similar among JRA-55, ERA-Interim, and MERRA-2, while the STT mass flux in MERRA-1 is at least 25% lower. In the other direction, TST mass flux totals are significantly higher in MERRA-1 ($\sim 51\%$) and MERRA-2 ($\sim 29\%$) compared to those from ERA-Interim and JRA-55.

Net STE is expected to be near zero, or balanced, over a long time period as a result of mass continuity. However, all reanalyses result in a net exchange that is either positive or negative (i.e. net TST or STT, respectively). Net mass fluxes in JRA-55 and ERA-Interim are both negative (STT-dominant), but the net flux amounts to only $\sim 4\%$ of the total flux (TST + STT). However, net mass fluxes in MERRA-1 and MERRA-2 are both positive and amount to about 33% and 12% of their total fluxes, respectively.

Table A.1 also includes the globally integrated mass fluxes of the four transport subcategories (i.e. vertical STT, vertical TST, lateral STT, and lateral TST). Net vertical STE fluxes are negative (STT-dominant) in JRA-55 and ERA-Interim, marginally negative in MERRA-2, and positive (TST-dominant) in MERRA-1. One unique commonality among the reanalyses is the net lateral flux. Each model shows a net positive net lateral STE mass flux. Although net lateral fluxes are unanimously positive, the MERRA-1/2 net fluxes are significantly larger than those in JRA-55 and ERA-Interim.

4.3 STE meridional distributions

Annually and zonally integrated latitudinal distributions of STE are shown in Fig. 8. Meridional distributions, similar to geographic distributions, demonstrate the latitudinal dependence of STE and offer a more quantitative comparison of the regional differences. Once again, we show both total STE and STE separated by the transport subcategories in the meridional distributions, but TST, STT, and net STE are superimposed in each distribution.

Total STE meridional distributions (Fig. 8a) show similar latitudinal variations in TST and STT in each model, but differences in the magnitude of each transport direction lead to large differences in net STE, especially in the extratropics. The meridional distributions for vertical (Fig. 8b) and lateral (Fig. 8c) subcategories demonstrate that the majority of these differences can be attributed to vertical STE, though lateral TST plays an important role in the subtropics and is clearly much larger in the MERRA reanalyses (especially in the NH).

4.4 Annual cycles

In addition to understanding regional differences in STE, examining differences in the seasonality of transport can be important for determining the significance of STE on UTLS composition throughout the year. Annual cycles of normalized STT and TST are presented in Fig. 9 and separated by hemisphere. Mass fluxes of STT and TST are normalized using the maximum and minimum monthly means over the 15-year period:

$$N_i = \frac{\overline{month}_i - MIN(\overline{month})}{MAX(\overline{month}) - MIN(\overline{month})} \quad (4.1)$$

Where, \overline{month}_i is the monthly mean for each month ($i = 1-12$) and N_i is now the i^{th} normalized monthly mean mass flux. Normalized STT mass fluxes are similar among the models in the NH and SH, but the hemispheres differ in the timing of annual minimum and maximum STT. Annual STT is at maximum and minimum in the late winter (DJF) and late summer (JJA) in the NH, while the maximum and minimum STT occur during early Autumn (MAM) and spring (SON) in the SH. One unique difference in STT is apparent during the Austral summer, where MERRA-2 normalized mass fluxes are considerably smaller during those months compared to the other reanalyses. Although the reanalyses show similar seasonality for STT, there are some differences in seasonal variability. While there are no uniform differences in variability within the hemispheres or among the reanalyses, the monthly variabilities are considerably larger in the SH than in the NH.

There are more apparent differences in the annual cycles of TST (middle row of Fig. 9). In particular, normalized TST mass flux in the NH reveals two preferred seasonal cycles amongst the models. In JRA-55 and ERA-Interim, the annual cycle of TST is weakly bimodal with maxima occurring during the NH winter (DJF) and summer (JJA). The MERRA reanalyses, on the other hand, are not bimodal and reach a maximum during the NH winter and a minimum during NH summer.

Although the TST annual cycle is inconsistent in the NH, TST seasonality in the SH is comparable in the reanalyses, with a maximum during the late summer and early fall (FMA) and minimum during the winter (JJA). Similar to STT, the TST annual cycles are more variable in the SH.

While the normalized annual cycles of TST and STT demonstrate the seasonality of STE, they do not represent amplitudes of the annual cycles (i.e. $MAX(\overline{month}) - MIN(\overline{month})$). Table A.2 provides annual cycle amplitudes for each hemisphere and reanalysis. JRA-55, ERA-Interim, and MERRA-2 largely agree on TST and STT annual cycle amplitudes in both hemispheres, with the exception of STT amplitudes in the SH. On the other hand, annual cycle amplitudes in MERRA-1, particularly in the NH, are larger for TST and smaller for STT compared to the other reanalyses.

Annual cycles of net STE are shown in the top row of Figure 10 and left un-normalized to show the combined effects of differences in seasonality and in dominance of STE pathway. Both MERRA reanalyses show a positive net cross-tropopause mass flux (TST) throughout their annual cycles in the NH. Alternatively, JRA-55 and ERA-Interim exhibit a NH seasonal cycle that is STT-dominant in the winter and early spring and TST dominant in the summer. In the SH, JRA-55 and ERA-Interim again show consistent seasonality, and are STT-dominant through most of the year and only briefly positive during the summertime (DJF). While similar in shape, MERRA-2 exhibits positive net exchange that spans all seasons but winter (JJA). MERRA-1, as in the NH, exhibits only positive net STE and a weaker annual cycle compared to the other reanalyses. The largest monthly net STE mass flux variability is found in the annual cycles of MERRA-1.

Annual cycles of the transport subcategories also reveal important differences in the seasonality of STE and the contribution of individual processes to the total annual cycles. Un-normalized net vertical and lateral annual cycles are also given

in Fig. 10 for both hemispheres. Generally, the seasonality of net vertical mass flux is similar in shape to the net annual cycle of total STE in each hemisphere, with a few important differences. Specifically, the net vertical STE annual cycle of MERRA-2 is shown to be STT-dominant during the NH wintertime, whereas the total net STE indicates positive net exchange through all seasons. The SH net vertical STE annual cycles are not significantly different from those represented by net total STE, aside from a negative shift (i.e., a greater influence of STT).

For annual cycles of lateral transport, all four reanalyses show similar seasonal behavior, with a minimum in late spring and early summer and a maximum during the late fall and early winter and are TST dominant in both hemispheres. Annual cycles of lateral transport in MERRA-1/2 have a slightly larger amplitude than those in ERA-Interim and JRA-55 and are displaced at higher net positive fluxes, which is consistent with the analyses presented in Sections (4.1 & 4.3) above.

4.5 STE time series

Time series of STE are examined over the 15-year period to further evaluate similarities and differences between the reanalysis models. In Fig. 11, global time series of STT and TST are shown and are normalized with respect to the mean STT and TST mass fluxes, respectively (i.e., mean fluxes are removed). STT throughout the period shows two modes of long-term changes in the reanalyses: increasing mass fluxes over time in JRA-55 and ERA-Interim and decreasing mass fluxes over time in the MERRA reanalyses. Similar long-term increases in TST can be seen in the ERA-Interim and JRA-55 time series. In the MERRA reanalyses, however, long-term changes in TST are shown to be largely increasing in MERRA-1 and near-zero in MERRA-2.

Vertical and lateral STE time series are shown in the middle and bottom rows of Fig. 11, respectively. Vertical STT shows similar patterns and variability to that from total STT for each reanalysis. Mainly, there are decreasing vertical STT mass fluxes in MERRA models and increasing fluxes in JRA-55 and ERA-Interim. In a similar manner, vertical TST is increasing over the period in ERA-Interim, JRA-55, slightly decreasing in MERRA-2, and strongly increasing in MERRA-1. Lateral STE time series for all reanalyses show little to no long-term variability. There is one exception, however, with lateral TST in MERRA-1 showing a potential long-term increase in mass flux.

The long-term increases and decreases in STE identified in Figure 11 are associated primarily with vertical STE and are considerably large relative to the mean, especially given the relatively short time period analyzed. In order to better understand the source of these changes we also analyzed time series of vertical STE occurring in extratropical and tropical domains. Based on the analyses presented thus far and conventional STE knowledge, vertical transport in the tropics is primarily upward (TST), while it is primarily downward (STT) in the extratropics (with the exception of MERRA-1). These geographically separated upward STE modes are largely the result of the BDC. Thus, we expect long-term changes in vertical TST in the tropics and vertical STT in the extratropics to be consistent. Figure 12 highlights these time series and the time series for the remaining modes (vertical STT in the tropics and TST in the extratropics) from each reanalysis.

In Figure 12, long-term changes in vertical STT are negligible in the tropics and apparent in the extratropics, while the opposite is true for vertical TST (except for MERRA-1). Specifically, JRA-55 and ERA-Interim show increasing vertical STT and TST in the extratropics and tropics, respectively, whereas MERRA-2 shows decreasing mass fluxes over the 15-year period.

The observed consistency in the sense of the long-term changes of vertical TST in the tropics and STT in the extratropics in ERA-Interim, JRA-55, and MERRA-2 suggests that changes in the BDC may be responsible for this behavior. Specifically, the increasing fluxes for tropical TST and extratropical STT over time in JRA-55 and ERA-Interim indicate an acceleration in the BDC. While the decreases in MERRA-2 indicate a deceleration of the BDC. Changes in the speed of the BDC have been examined in previous studies. In particular, decreases in tropical stratospheric water vapor, ozone, and temperature observed by satellite correspond to an increase in tropical upwelling associated with an enhanced BDC (Randel et al., 2006). Chemistry-climate models have also indicated an acceleration of the BDC over time (e.g., Austin and Li, 2006). These previous observational and modeling studies are consistent with the results from ERA-Interim and JRA-55 here, while MERRA-2 is in disagreement and MERRA-1 does not indicate changes in the BDC over time.

4.6 Reanalysis model evaluations

This paper is largely a comparison of STE estimates using multiple state-of-the-art reanalysis models, but we also briefly evaluate some model differences through various metrics and diagnostics here. The goal is to provide general context and logical reasoning to explain some of the aforementioned STE variations among the reanalyses.

4.6.1 STE occurrence geographic distributions

In order to assess quantitative and qualitative STE differences, particularly the larger differences found for TST, we have to consider whether the frequency of STE events differs among the models. Evaluating STE occurrence frequency in each reanalysis informs us whether the amount of STE is a result of more frequent STE or differences in the magnitude of transport in individual events.

In Fig. 13, total STT and TST occurrence frequencies are shown. There are noticeable differences between the ERA-Interim and JRA-55 pair and the MERRA reanalyses. In particular, ERA-Interim and JRA-55 show higher occurrence frequencies globally for STT, while the MERRA occurrence frequencies are higher for TST. Taken together with the results from the geographic distributions of STE mass flux (Figs. 4–7), these analyses suggest that differences in mass flux between the reanalyses are largely the result of differences in the frequency of exchange events.

4.6.2 Diagnostics

The differences in STE occurrence and mass flux estimates among the models, to some extent, are due to dynamical and/or physical differences between the models. Over a long period these small differences may result in considerable variations in climatological evaluations of STE. Dynamical differences may include offsets in the locations of upper tropospheric jet streams or the strength of circulations including the vertical motion. Physical differences include offsets in the altitude of the tropopause or the location of the tropopause break.

These dynamical and physical characteristics can impact a reanalysis model's long-term representation of STE. For example, differences in vertical STE can be the result of higher or lower tropopause altitudes among the models. Assuming the

dynamics are equivalent in each model, differences in the altitude of the tropopause imply that different elements of the dynamical features are analyzed for transport calculations, which would ultimately lead to differences in STE estimates. A similar argument can be made for uniform tropopause altitudes and dynamical differences.

Because the largest differences in our comparison are those associated with vertical STE, comparing the magnitudes of vertical motion at and in a layer closely above and below the tropopause may reveal a dynamical source of transport differences. However, we find that probability distributions of vertical motion are quite similar among all the reanalyses (not shown).

Alternative dynamical and physical differences amongst the reanalyses outlined above can be assessed using tropopause break-relative zonal means of tropopause altitudes and horizontal wind speeds. Tropopause break-relative zonal means are computed separately for each hemisphere using a relative latitude coordinate at each longitude grid point, where the latitude of the tropopause break (location where tropopause pressure is 150 hPa) is subtracted from the model latitude grid. Once the relative latitude grid is known for each longitude in a hemisphere, zonal means are calculated in relative latitude and on a dense, regularly spaced pressure level grid in the vertical dimension. Figure 14 shows a single month of these tropopause break-relative zonal means from each reanalysis for a cross-section that includes both hemispheres and limits the vertical dimension to altitudes in the UTLS. In this case, the relative grids in each hemisphere are centered at the mean latitude of the tropopause break so that the zonal mean represents typical conditions in each hemisphere. It is important to compute zonal means in this manner since dynamical and physical differences in traditional Eulerian means may be overly smoothed and therefore less informative about the typical collocations of the jets and tropopause altitudes and the magnitudes of each.

In Figure 14, it is apparent that extratropical and tropical tropopause altitudes in both MERRA reanalyses are uniformly higher than those in both JRA-55 and ERA-Interim. This alone may be an important contributor to STE differences between the reanalyses. Slight offsets in the locations of the subtropical jets indicate that there are also dynamical differences that may contribute to differences in STE. Although we limit this analysis to a single month here, it is important to note that the differences shown in Figure 14 are consistent throughout the analysis period.

Chapter 5

Conclusions and discussion

In this study, we examined global characteristics of STE over a 15-year period (1996-2010) using a trajectory model and output from multiple reanalyses: ERA-Interim, JRA-55, MERRA-2, and MERRA-1. STE was separated into four sub-categories in an attempt to isolate known transport processes: vertical STT, vertical TST, lateral STT, and lateral TST. Vertical STE was further separated into domains being either extratropical or tropical based upon the altitude of the tropopause.

5.1 Principal conclusions

This study, in contrast to the vast majority of previous work, used the lapse-rate tropopause or LRT as the troposphere-stratosphere boundary rather than an isosurface of potential vorticity (PV) or dynamic tropopause. In order to demonstrate the impact of this choice for STE studies, we presented a comparison of STE estimates using the LRT method and results from a recent study that used a dynamic tropopause (Škerlak et al., 2014). We found that:

1. magnitudes of STE are uniformly smaller using the LRT,

2. spatial placement and variability of STT is similar between methods, and
3. spatial placement and variability of TST is largely different, with the most significant differences found in the polar regions.

These differences correspond to a change in the net transport direction in the polar regions when using the LRT (i.e., downward or STT-dominant rather than upward). Such net transport at high latitudes from the LRT method is more consistent with our established understanding of UTLS dynamics: net upward motion in the tropics and net downward in the extratropics and polar regions.

The main focus of this paper was not a method comparison, but a comparison of STE among four state-of-the-art atmospheric reanalyses. Doing so, we stratified transport into several categories in order to investigate the STE climatologies both quantitatively and qualitatively. It was found that the models can be grouped into two populations: STT-dominant and TST-dominant (Table A.1). JRA-55 and ERA-Interim are STT-dominant, while the MERRA reanalyses are both TST-dominant. The net transport in the STT-dominant reanalyses, however, is small relative to the total transport, while the opposite is true for the TST-dominant reanalyses.

Geographic distributions and zonal mean latitudinal distributions revealed important characteristics about the two reanalysis populations. Notably, the largest differences were found in the extratropics and associated primarily with vertical STE. Geographic distributions of STT maxima were similar amongst all reanalyses, while the opposite was true for TST. MERRA-1 was typically an outlier relative to the remaining reanalyses, but similar differences (though largely diminished) were found between MERRA-2 and the STT-dominant reanalyses (ERA-Interim and JRA-55). Lateral STE was found to be consistent geographically with prior studies of Rossby wave breaking events along the tropopause break (Postel and Hitchman, 1999; Homeyer and Bowman, 2013). Although geographic placement

and net transport for lateral STE was consistent among the models, the MERRA reanalyses showed roughly twice the magnitude of net poleward transport (i.e., TST).

Seasonality of STE amongst the reanalyses was also found to be similar for some transport categories and directions and significantly different for others. Similar to geographic consistencies observed, we found that STT seasonality is consistent among the reanalyses and in both hemispheres. However, annual cycles of TST in the NH were found to be weakly bimodal in STT-dominant reanalyses and unimodal in the TST-dominant reanalyses, with smaller differences in the SH. Larger differences were found for annual cycles of net STE from the reanalyses, with MERRA-1 showing little seasonality in each hemisphere. Differences in net STE were shown to be associated primarily with vertical STE, which was a consistent outcome of all analyses.

Long-term changes were also investigated using time series analysis over the 15-year study period. These analyses indicated gradual increases and decreases in STT and TST mass flux for the STT-dominant models and MERRA-2, respectively. Further analyses of the transport subcategories suggested that long-term changes in total STE are associated with either an acceleration or deceleration of the BDC. Specifically, the BDC is apparently decelerating in MERRA-2 and accelerating in JRA-55 and ERA-Interim from 1996–2010.

Finally, several diagnostics were applied to the reanalyses in order to shed light on the sources of the STE differences. We found that differences in transport are likely the result of differences in the frequency of irreversible STE rather than the magnitude of individual events. We also found there to be persistent offsets in the altitude of the tropopause and the locations of upper-tropospheric jets between the STT-dominant and TST-dominant models. These dynamical and physical

differences are considerable regarding the climatological STE differences, both of which likely contribute some to the observed STE differences.

5.2 Discussion

The analyses in this study demonstrate that while there are some areas of agreement in the magnitude, geographic distribution, and frequency of large-scale STE, there are important differences that can lead to varying conclusions of the impact of STE on UTLS composition, the radiation budget, and climate. While this study is the first model comparison of global STE over a long time period, there are some limitations that could be improved in future work to shed further light on these differences. First, the analysis time period could be increased. Each reanalysis model used in this study has output available from 1979 to 2015, roughly 2.5 times longer than that used here. Expanding the analysis period may provide more knowledge on the statistical behavior regarding the long-term changes associated with the BDC (Section 4.5). An extended analysis period may also reduce variability in the seasonality and regional distributions analyzed here and thus increase confidence in the results.

Second, while the present generation of the reanalysis models are significant advancements for studies of UTLS dynamics and associated processes over previous generations, model improvements can still be made in the UTLS. Given the limited spatiotemporal observations of STE available, it is understandable that model simulations of transport could differ considerably. However, some of these differences are likely related to basic model choices such as grid resolution. For example, the vertical grids are nearly equivalent in ERA-Interim and JRA-55, which differ considerably from that used in MERRA-1/2. Notably, vertical resolution is finer at levels below the tropical tropopause in ERA-Interim and JRA-55, but finer above the tropical tropopause in the MERRA Reanalyses. Since the vertical grid

resolution and placement of vertical grid levels in the UTLS may have important impacts on tropopause-relative analyses such as STE (especially since current vertical resolution of reanalyses in the UTLS is 1 km), it is important to understand the sensitivity of such analyses to this model design choice.

Third, although we use kinematic output (ω ; hPa s⁻¹) to vertically advect parcel trajectories, it is possible to use diabatic (heating rates; K s⁻¹) output instead. Because kinematic vertical velocities are derived using mass continuity, small numerical errors can occur. Diabatic heating and cooling rates, on the other hand, represent physical vertical motion and are less prone to numerical errors. To briefly illustrate the sensitivity to vertical velocity output, we constructed a climatology of STE using diabatic output from JRA-55 and compared it to kinematic geographic distributions and STE occurrence (Figure 15). The comparison shows a decrease in TST mass flux magnitudes and occurrence. While diabatic vertical velocities diminish some error, they are typically slower than kinematic vertical velocities. Thus, using diabatic output may require modification to our STE algorithm: allow 48–72 hours for initial STE identification, as diabatic vertical motion is generally weaker. It is apparent that further investigation is necessary to provide an adequate understanding of a diabatically driven STE.

Furthermore, while this study compared STE among reanalyses and attempted to diagnose potential sources of those differences, much more work can be done to examine them. Such analyses may lead to future improvements in the models, especially in the UTLS.

Bibliography

- Appenzeller, C., J. R. Holton, and K. H. Rosenlof, 1996: Seasonal variation of mass transport across the tropopause. *J. Geophys. Res.*, **101 (D10)**, doi:10.1029/96JD00821.
- Austin, J. and F. Li, 2006: On the relationship between the strength of the Brewer-Dobson circulation and the age of stratospheric air. *Geophys. Res. Lett.*, **33 (17)**, doi:10.1029/2006GL026867.
- Birner, T., 2010: Recent widening of the tropical belt from global tropopause statistics: Sensitivities. *J. Geophys. Res.*, **115 (D23)**, doi:10.1029/2010JD014664.
- Bosilovich, M. G., et al., 2015: MERRA-2; Initial Evaluation of the Climate. *Technical Report Series on Global Modeling and Data Assimilation*, **43**.
- Bowman, K. P., 1993: Large-scale isentropic mixing properties of the antarctic polar vortex from analyzed winds. *J. Geophys. Res.*, **98 (D12)**, 23 013–23 027, doi:10.1029/93JD02599.
- Bowman, K. P. and G. D. Carrie, 2002: The mean-meridional transport circulation of the troposphere in an idealized GCM. *J. Atmos. Sci.*, **59 (9)**, 1502–1514, doi:10.1175/1520-0469(2002)059<1502:TMMTCO>2.0.CO;2.
- Brewer, A., 1949: Evidence for a world circulation provided by the measurements of helium and water vapour distribution in the stratosphere. *Quart. J. Roy. Meteorol. Soc.*, **75 (326)**, 351–363, doi:10.1002/qj.49707532603.
- Cooper, O., et al., 2004: On the life cycle of a stratospheric intrusion and its dispersion into polluted warm conveyor belts. *J. Geophys. Res.*, **109 (D23)**, doi:10.1029/2003JD004006.
- Danielsen, E. F., 1968: Stratospheric-tropospheric exchange based on radioactivity, ozone and potential vorticity. *J. Atmos. Sci.*, **25 (3)**, 502–518, doi:10.1175/1520-0469(1968)025<0502:STEBOR>2.0.CO;2.
- Dee, D., et al., 2011: The ERA-Interim reanalysis: Configuration and performance of the data assimilation system. *Quart. J. Roy. Meteorol. Soc.*, **137 (656)**, 553–597, doi:10.1002/qj.828.

- Dobson, G. M. B., 1956: Origin and distribution of the polyatomic molecules in the atmosphere. *Proceedings of the Royal Society of London. Series A, Mathematical and Physical Sciences*, **236 (1205)**, 187–193, URL <http://www.jstor.org/stable/100027>.
- Ertel, H. and C.-G. Rossby, 1949: A new conservation-theorem of hydrodynamics. *Geofisica pura e applicata*, **14 (3)**, 189–1936, doi:10.1007/BF01981973.
- Forster, P. M. d. F. and K. P. Shine, 2002: Assessing the climate impact of trends in stratospheric water vapor. *Geophys. Res. Lett.*, **29 (6)**, 10–1–10–4, doi:10.1029/2001GL013909.
- Gottelman, A., P. Hoor, L. Pan, W. Randel, M. Hegglin, and T. Birner, 2011: The extratropical upper troposphere and lower stratosphere. *Rev. Geophys.*, **49 (3)**, doi:10.1029/2011RG000355.
- Gottelman, A. and A. H. Sobel, 2000: Direct diagnoses of stratosphere-troposphere exchange. *J. Atmos. Sci.*, **57 (1)**, 3–16, doi:10.1175/1520-0469(2000)057<0003:DDOSTE>2.0.CO;2.
- Holton, J. R., P. H. Haynes, M. E. McIntyre, A. R. Douglass, R. B. Rood, and L. Pfister, 1995: Stratosphere-troposphere exchange. *Rev. Geophys.*, **33 (4)**, 403–439, doi:10.1029/95RG02097.
- Homeyer, C. R. and K. P. Bowman, 2013: Rossby wave breaking and transport between the tropics and extratropics above the subtropical jet. *J. Atmos. Sci.*, **70 (2)**, 607–626, doi:10.1175/JAS-D-12-0198.1.
- Keyser, D. and M. Shapiro, 1986: A review of the structure and dynamics of upper-level frontal zones. *Mon. Weather Rev.*, **114 (2)**, 452–499, doi:10.1175/1520-0493(1986)114<0452:AROTSA>2.0.CO;2.
- Kobayashi, S., et al., 2015: The JRA-55 reanalysis: general specifications and basic characteristics. *J. Meteorol. Soc. Japan*, **93 (1)**, 5–48, doi:10.2151/jmsj.2015-001.
- Kunz, A., P. Konopka, R. Müller, and L. Pan, 2011: Dynamical tropopause based on isentropic potential vorticity gradients. *J. Geophys. Res.*, **116 (D1)**, doi:10.1029/2010JD014343.
- Lacis, A. A., D. J. Wuebbles, and J. A. Logan, 1990: Radiative forcing of climate by changes in the vertical distribution of ozone. *J. Geophys. Res.*, **95 (D7)**, 9971–9981, doi:10.1029/JD095iD07p09971.
- Lamarque, J.-F. and P. G. Hess, 1994: Cross-tropopause mass exchange and potential vorticity budget in a simulated tropopause folding. *J. Atmos. Sci.*, **51 (15)**, 2246–2269, doi:10.1175/1520-0469(1994)051<2246:CTMEAP>2.0.CO;2.

- Lin, M., et al., 2012: Springtime high surface ozone events over the western United States: Quantifying the role of stratospheric intrusions. *J. Geophys. Res.*, **117** (D21), doi:10.1029/2012JD018151.
- Palmén, E., 1948: On the distribution of temperature and wind in the upper westerlies. *J. Meteor.*, **5** (1), 20–27, doi:10.1175/1520-0469(1948)005<0020:OTDOTA>2.0.CO;2.
- Pan, L., W. Randel, B. Gary, M. Mahoney, and E. J. Hints, 2004: Definitions and sharpness of the extratropical tropopause: A trace gas perspective. *J. Geophys. Res.*, **109** (D23), doi:10.1029/2004JD004982.
- Postel, G. A. and M. H. Hitchman, 1999: A climatology of Rossby wave breaking along the subtropical tropopause. *J. Atmos. Sci.*, **56** (3), 359–373, doi:10.1175/1520-0469(1999)056<0359:ACORWB>2.0.CO;2.
- Price, J. and G. Vaughan, 1993: The potential for stratosphere-troposphere exchange in cut-off-low systems. *Quart. J. Roy. Meteorol. Soc.*, **119** (510), 343–365, doi:10.1002/qj.49711951007.
- Randel, W. J., M. Park, L. Emmons, D. Kinnison, P. Bernath, K. A. Walker, C. Boone, and H. Pumphrey, 2010: Asian monsoon transport of pollution to the stratosphere. *Science*, **328** (5978), 611–613, doi:10.1126/science.1182274.
- Randel, W. J., D. J. Seidel, and L. L. Pan, 2007: Observational characteristics of double tropopauses. *J. Geophys. Res.*, **112** (D7), doi:10.1029/2006JD007904.
- Randel, W. J., F. Wu, H. Vömel, G. E. Nedoluha, and P. Forster, 2006: Decreases in stratospheric water vapor after 2001: Links to changes in the tropical tropopause and the Brewer-Dobson circulation. *J. Geophys. Res.*, **111** (D12), doi:10.1029/2005JD006744.
- Reutter, P., B. Škerlak, M. Sprenger, and H. Wernli, 2015: Stratosphere-troposphere exchange (STE) in the vicinity of North Atlantic cyclones. *Atmos. Chem. Phys.*, **15** (19), 10 939–10 953, doi:10.5194/acp-15-10939-2015.
- Rienecker, M. M., et al., 2011: MERRA: NASA’s modern-era retrospective analysis for research and applications. *J. Climate*, **24** (14), 3624–3648, doi:10.1175/JCLI-D-11-00015.1.
- Sawyer, J., 1956: The vertical circulation at meteorological fronts and its relation to frontogenesis. *Proceedings of the Royal Society of London A: Mathematical, Physical and Engineering Sciences*, **234** (1198), 346–362, doi:10.1098/rspa.1956.0039.
- Scott, R. and J. Cammas, 2002: Wave breaking and mixing at the subtropical tropopause. *J. Atmos. Sci.*, **59** (15), 2347–2361, doi:10.1175/1520-0469(2002)059<2347:WBAMAT>2.0.CO;2.

- Seo, K. and K. P. Bowman, 2001: A climatology of isentropic cross-tropopause exchange. *J. Geophys. Res.*, **106** (D22), 28–159.
- Seo, K.-H. and K. P. Bowman, 2002: Lagrangian estimate of global stratosphere-troposphere mass exchange. *J. Geophys. Res.*, **107** (D21), doi:10.1029/2002JD002441.
- Shapiro, M., 1980: Turbulent mixing within tropopause folds as a mechanism for the exchange of chemical constituents between the stratosphere and troposphere. *J. Atmos. Sci.*, **37** (5), 994–1004, doi:10.1175/1520-0469(1980)037<0994:TMWTFA>2.0.CO;2.
- Shapiro, M., 1981: Frontogenesis and geostrophically forced secondary circulations in the vicinity of jet stream-frontal zone systems. *J. Atmos. Sci.*, **38** (5), 954–973, doi:10.1175/1520-0469(1981)038<0954:FAGFSC>2.0.CO;2.
- Shapiro, M. and P. Kennedy, 1981: Research aircraft measurements of jet stream geostrophic and ageostrophic winds. *J. Atmos. Sci.*, **38** (12), 2642–2652, doi:10.1175/1520-0469(1981)038<2642:RAMOJS>2.0.CO;2.
- Škerlak, B., M. Sprenger, and H. Wernli, 2014: A global climatology of stratosphere–troposphere exchange using the ERA-Interim data set from 1979 to 2011. *Atmos. Chem. Phys.*, **14** (2), 913–937, doi:10.5194/acp-14-913-2014.
- Sprenger, M. and H. Wernli, 2003: A Northern Hemispheric climatology of cross-tropopause exchange for the ERA15 time period (1979–1993). *J. Geophys. Res.*, **108** (D12), doi:10.1029/2002JD002636.
- Stohl, A., 2001: A 1-year Lagrangian “climatology” of airstreams in the northern hemisphere troposphere and lowermost stratosphere. *J. Geophys. Res.*, **106** (30), 445–30, doi:10.1029/2000JD900570.
- Waugh, D. W. and L. M. Polvani, 2000: Climatology of intrusions into the tropical upper troposphere. *Geophys. Res. Lett.*, **27** (23), 3857–3860, doi:10.1029/2000GL012250.
- Wei, M.-Y., 1987: A new formulation of the exchange of mass and trace constituents between the stratosphere and troposphere. *J. Atmos. Sci.*, **44** (20), 3079–3086, doi:10.1175/1520-0469(1987)044<3079:ANFOTE>2.0.CO;2.
- Wernli, B. H. and H. C. Davies, 1997: A Lagrangian-based analysis of extratropical cyclones. I: The method and some applications. *Quart. J. Roy. Meteorol. Soc.*, **123** (538), 467–489, doi:10.1002/qj.49712353811.
- Wernli, H. and M. Bourqui, 2002: A Lagrangian “1-year climatology” of (deep) cross-tropopause exchange in the extratropical northern hemisphere. *J. Geophys. Res.*, **107** (D2), doi:10.1029/2001JD000812.

Wirth, V. and J. Egger, 1999: Diagnosing extratropical synoptic-scale stratosphere-troposphere exchange: A case study. *Quart. J. Roy. Meteorol. Soc.*, **125** (554), 635–655, doi:10.1002/qj.49712555413.

World Meteorological Organization (WMO), 1957: Definition of the tropopause. *WMO Bull.*, **6**, 136.

Appendix A

Figures & Tables

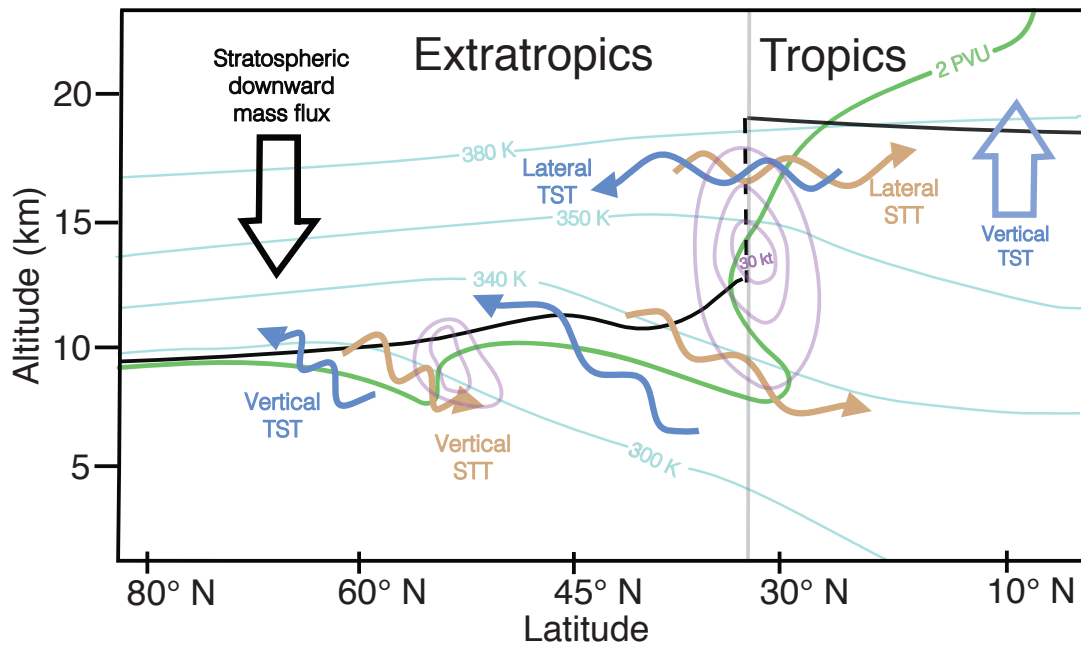


Figure 1: Schematic of STE identification method. Vertical STT and TST are shown by orange and blue arrows, respectively. Bold and wavy arrows represent Brewer–Dobson circulation and quasi-isentropic mixing processes, respectively. Potential temperature surfaces are given by the cyan lines, the lapse-rate tropopause by the black lines, and the 2 pvu PV isosurface by the green line. The solid gray line, coincident with the tropopause break (dashed black line), represents the boundary between the tropics and extratropics. Subtropical and polar jet streams are shown by solid purple isotachs.

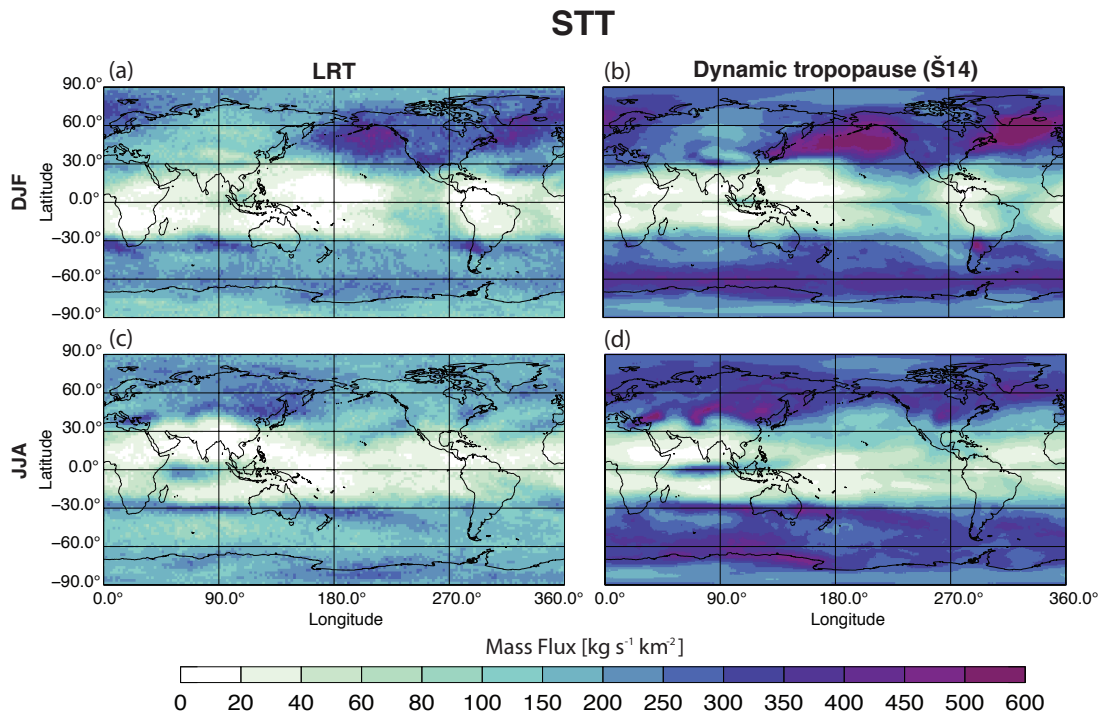


Figure 2: December, January, and February (DJF, top row) and June, July, and August (JJA, bottom row) mean STT mass fluxes for 1996–2010 using the lapse-rate tropopause method (left) and 1979–2011 using the dynamic tropopause method (right; from Škerlak et al. (2014)).

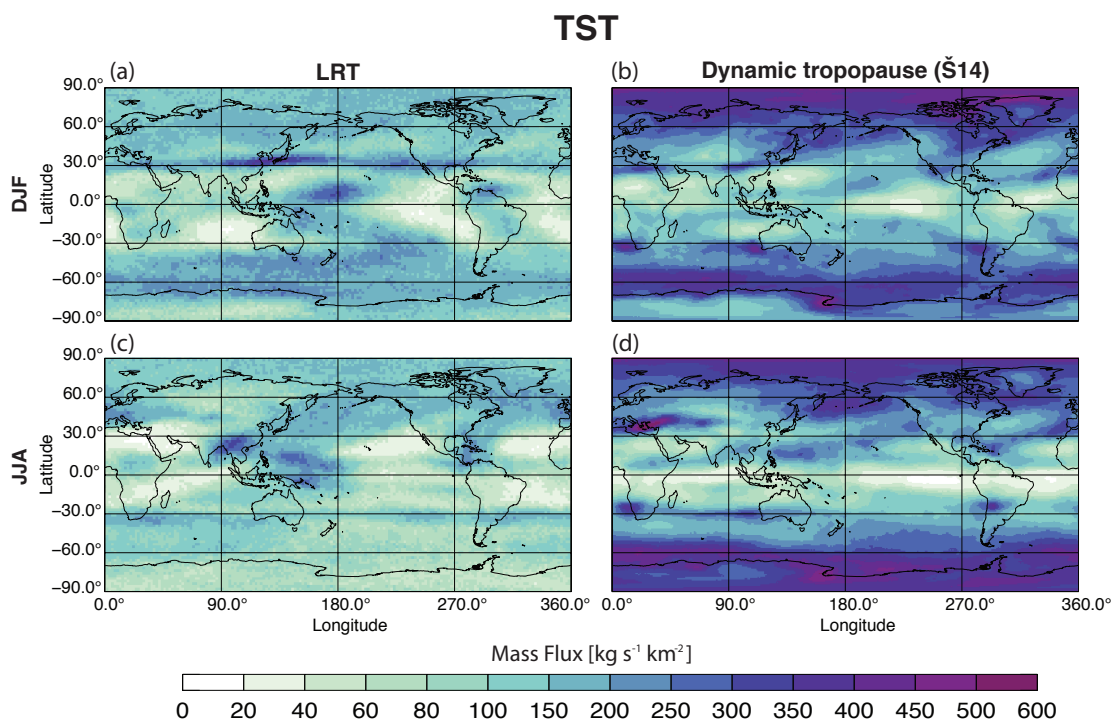


Figure 3: As in Fig. 2, but for TST.

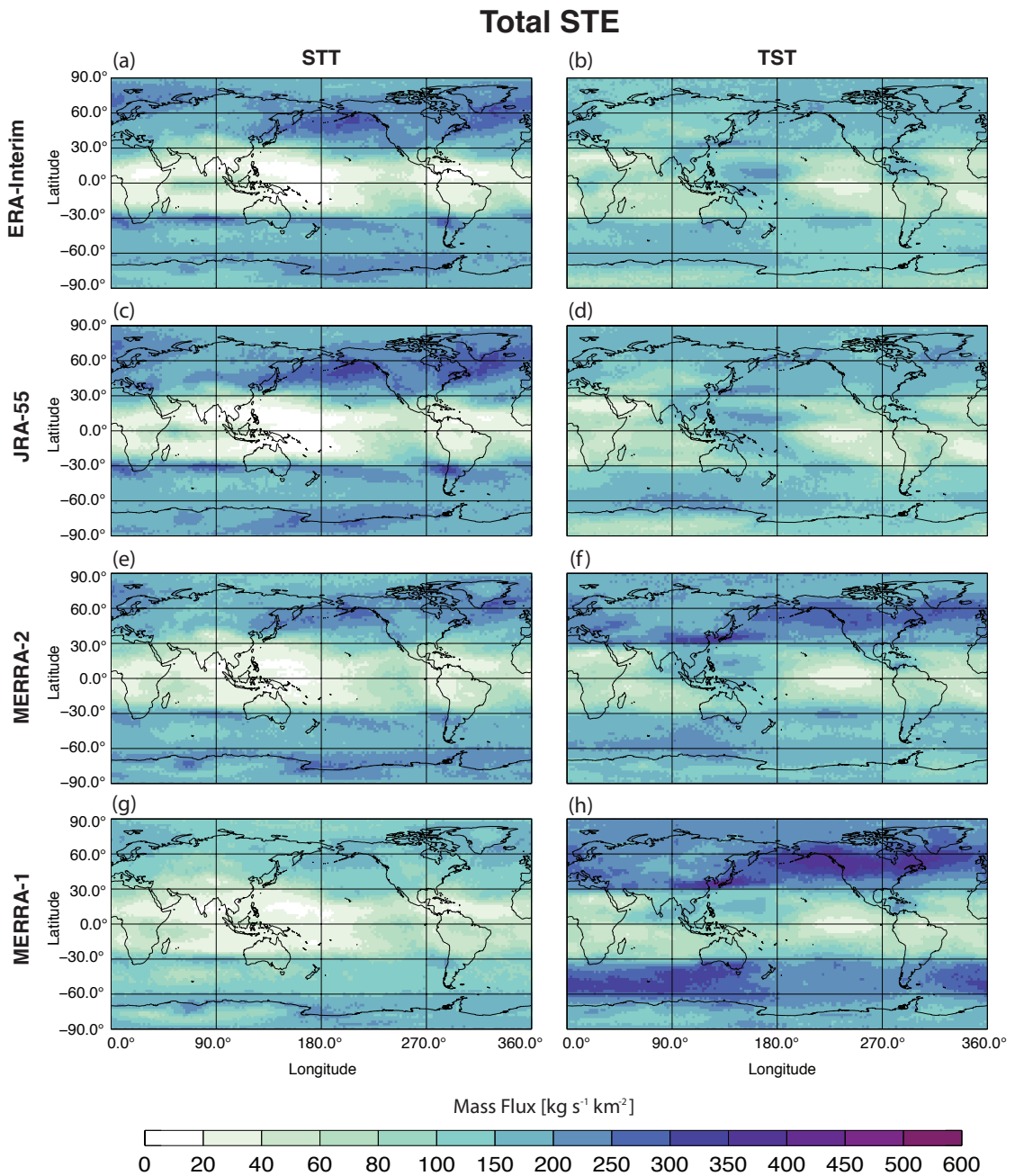


Figure 4: Annual mean geographic distributions of total STE mass flux for ERA-Interim (a & b), JRA-55 (c & d), MERRA-2 (e & f), and MERRA-1 (g & h). STE is separated into STT (left) and TST (right) for each reanalysis.

Vertical STE (extratropics)

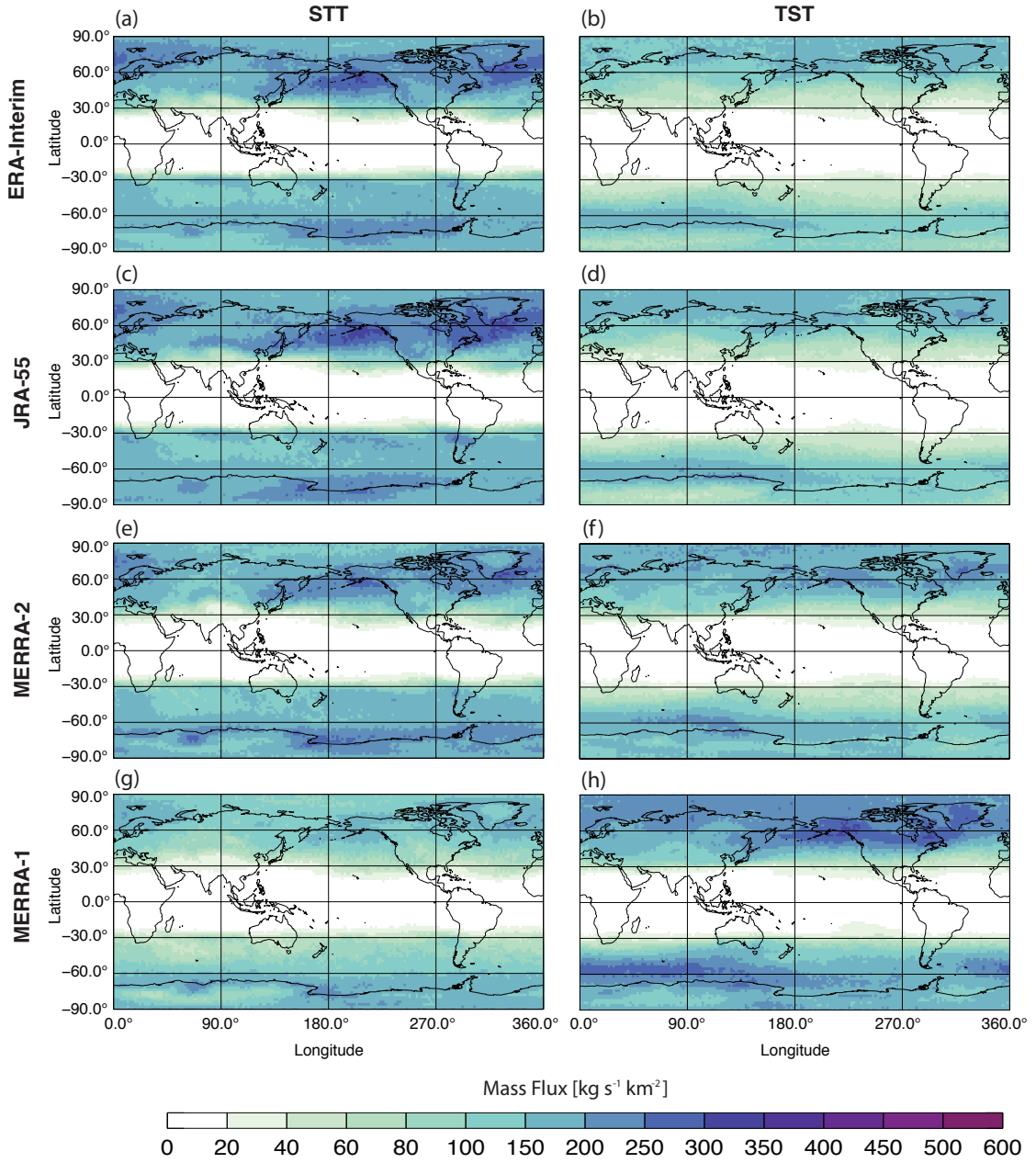


Figure 5: As in Fig. 4, but for vertical STE in the extratropics.

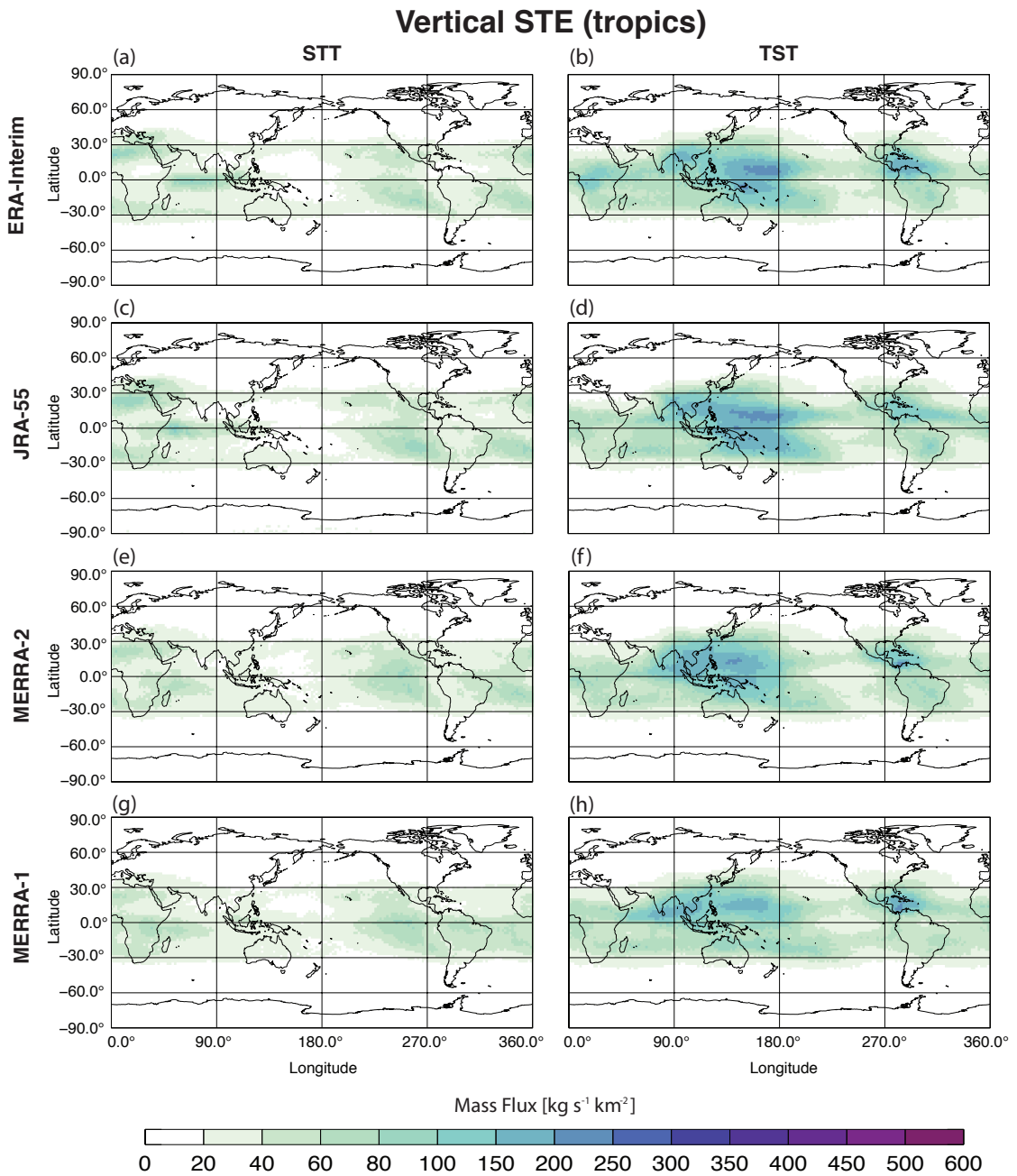


Figure 6: As in Fig. 4, but for the vertical STE in the tropics.

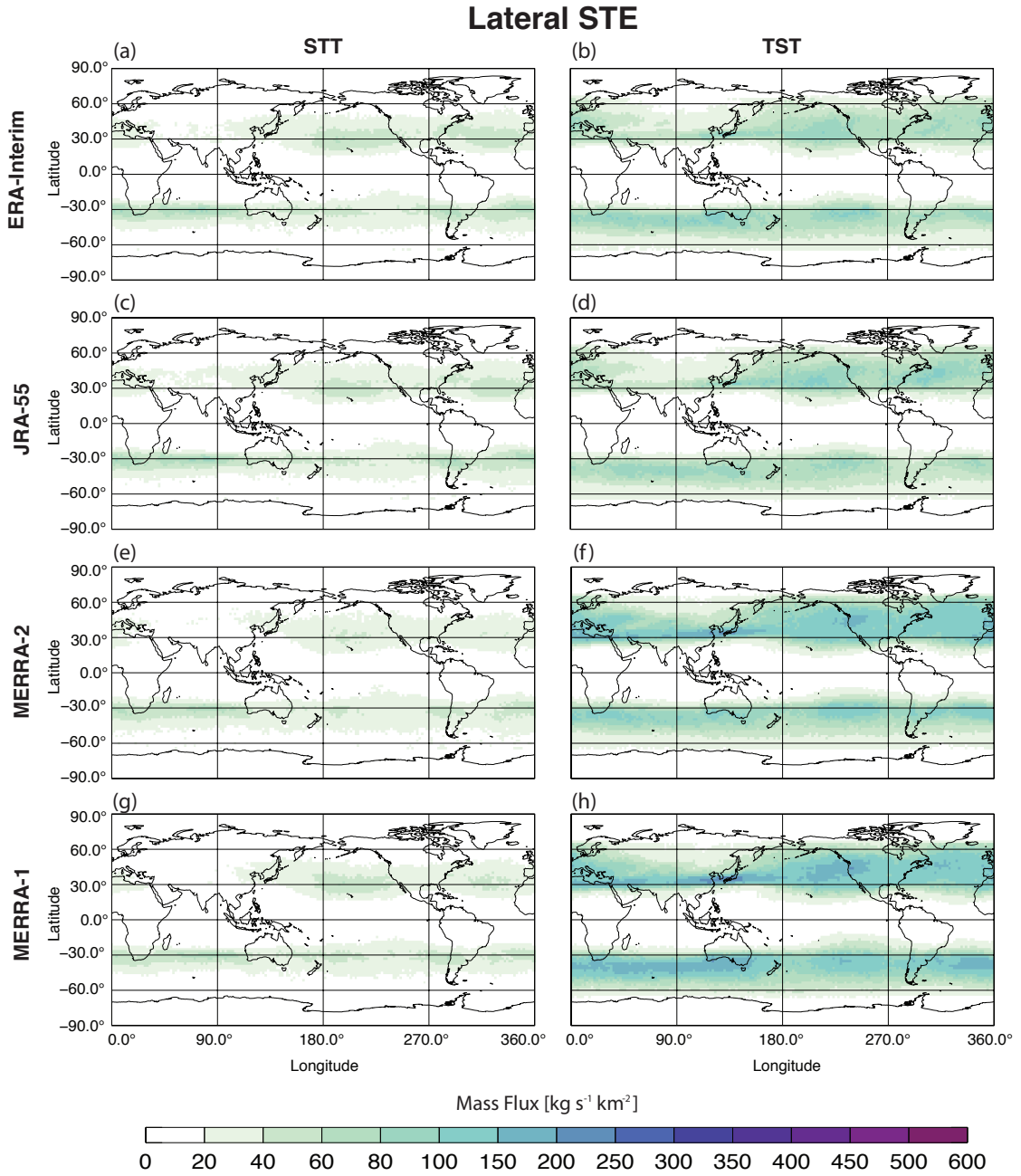


Figure 7: As in Fig. 4, but for lateral STE.

Table A.1: Globally integrated STE mass fluxes averaged over the 15-yr period for each reanalysis model. STT, TST, net (TST-STT), and gross (TST+STT) mass fluxes are given for each transport category (i.e. total, vertical, and lateral exchange). All mass flux units are $10^{10} \text{ kg s}^{-1}$.

| Total STE | | | | |
|-------------------|------------------------|------------------------|------------------------|--------------------------|
| Reanalyses | STT_T | TST_T | Net_T | Gross_T |
| JRA-55 | 5.83 | 5.29 | -0.54 | 11.12 |
| ERA-Interim | 5.56 | 5.10 | -0.47 | 10.66 |
| MERRA-2 | 5.16 | 6.57 | 1.41 | 11.73 |
| MERRA-1 | 3.86 | 7.74 | 3.88 | 11.60 |

| Vertical STE | | | | |
|---------------------|------------------------|------------------------|------------------------|--------------------------|
| Reanalyses | STT_V | TST_V | Net_V | Gross_V |
| JRA-55 | 5.29 | 4.10 | -1.19 | 9.39 |
| ERA-Interim | 5.02 | 3.86 | -1.16 | 8.88 |
| MERRA-2 | 4.69 | 4.68 | -0.012 | 9.37 |
| MERRA-1 | 3.39 | 5.55 | 2.16 | 8.94 |

| Lateral STE | | | | |
|--------------------|------------------------|------------------------|------------------------|--------------------------|
| Reanalyses | STT_L | TST_L | Net_L | Gross_L |
| JRA-55 | 0.54 | 1.19 | 0.65 | 1.73 |
| ERA-Interim | 0.55 | 1.24 | 0.69 | 1.79 |
| MERRA-2 | 0.47 | 1.89 | 1.42 | 2.36 |
| MERRA-1 | 0.47 | 2.19 | 1.72 | 2.66 |

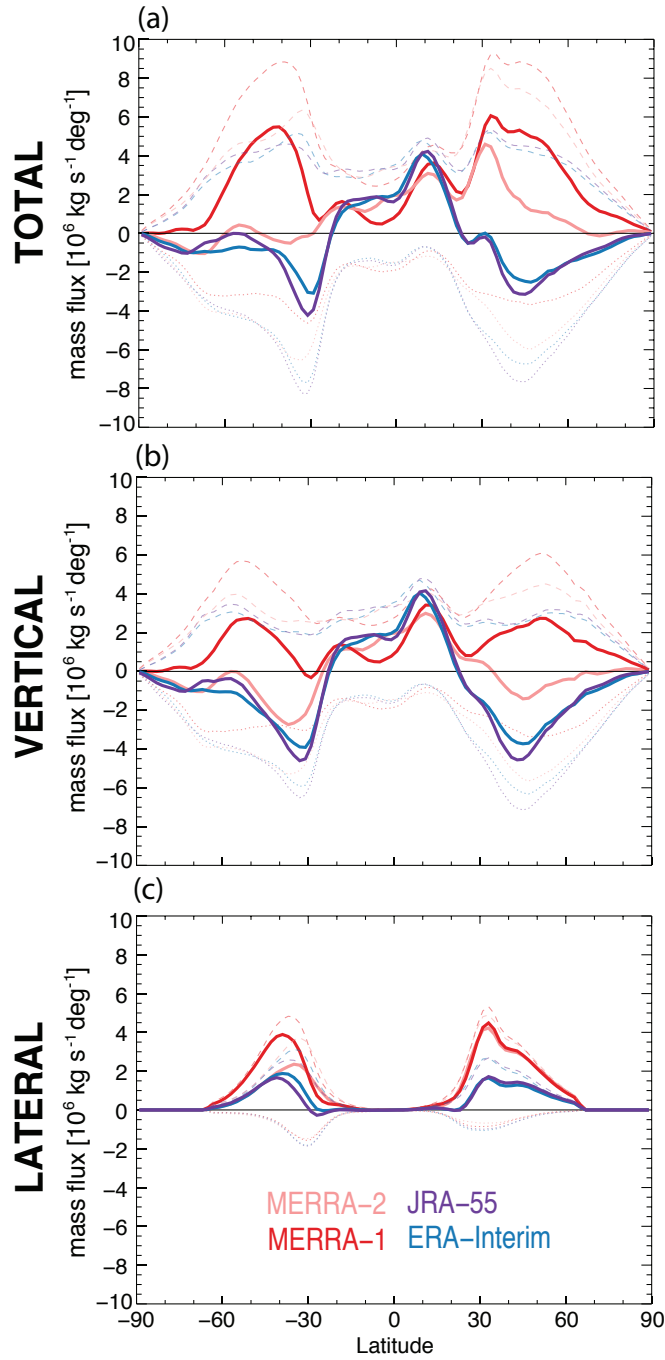


Figure 8: Annually and zonally averaged meridional distributions of STE from each reanalysis function of latitude and for (a) total STE, (b) vertical STE, and (c) lateral STE. STT is shown as the dotted lines (negative), TST as the dashed lines (positive), and the net transport is given by the solid lines in each panel. STE from JRA-55 is shown by the purple lines, ERA-Interim by the blue lines, and MERRA-2 and MERRA-1 by the light and dark red lines, respectively.

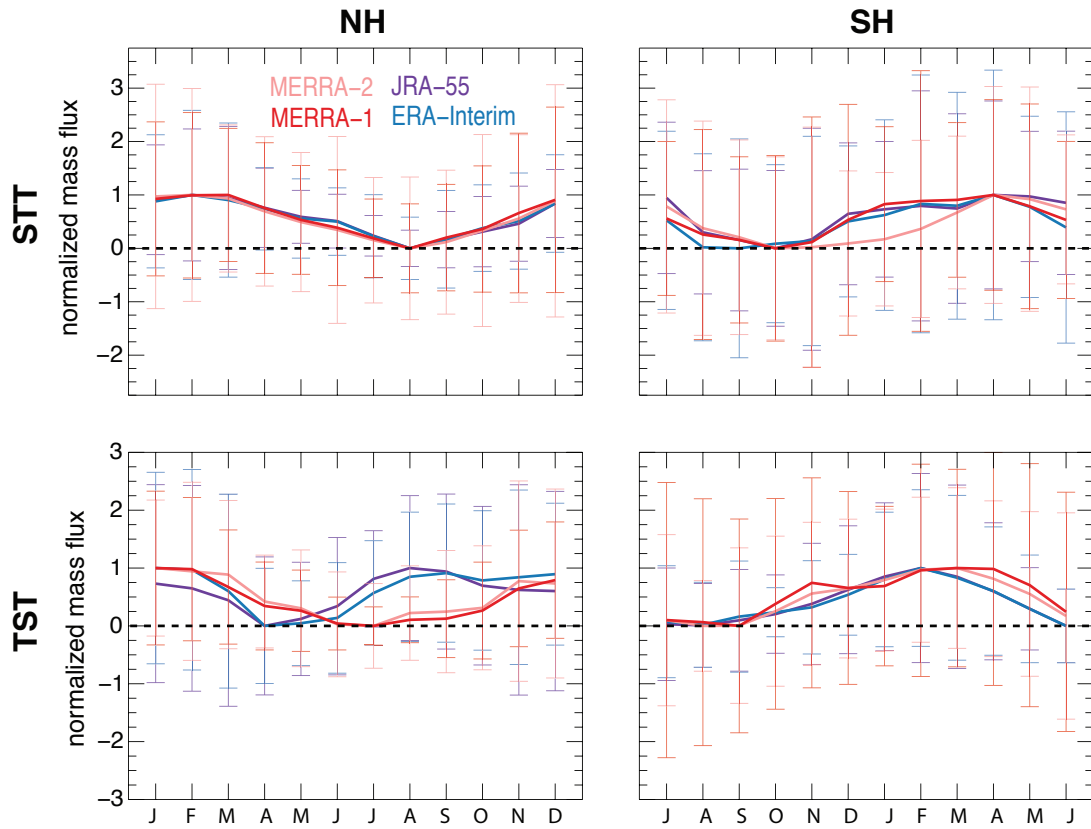


Figure 9: Annual cycles of (top row) normalized STT and (bottom row) normalized TST for the (left) Northern Hemisphere and (right) Southern Hemisphere from each reanalysis model. In each plot, the solid colored lines are the mean annual cycles and the colored error bars are plus/minus one standard deviation from the mean. STE from JRA-55 is shown by the purple lines, ERA-Interim by the blue lines, and MERRA-2 and MERRA-1 by the light and dark red lines, respectively. Note that SH and NH annual cycles are offset by 6 mo.

Table A.2: STT and TST annual cycle amplitudes given in both hemispheres from each reanalysis model. All amplitudes are in units of 10^9 kg s^{-1} .

| Reanalysis | STT | | TST | |
|-------------------|------------|-------|------------|------|
| | NH | SH | NH | SH |
| JRA-55 | 6.00 | 12.92 | 12.11 | 4.91 |
| ERA-Interim | 5.33 | 10.68 | 12.74 | 3.90 |
| MERRA-2 | 5.46 | 12.92 | 14.19 | 5.94 |
| MERRA-1 | 10.82 | 10.47 | 9.83 | 6.37 |

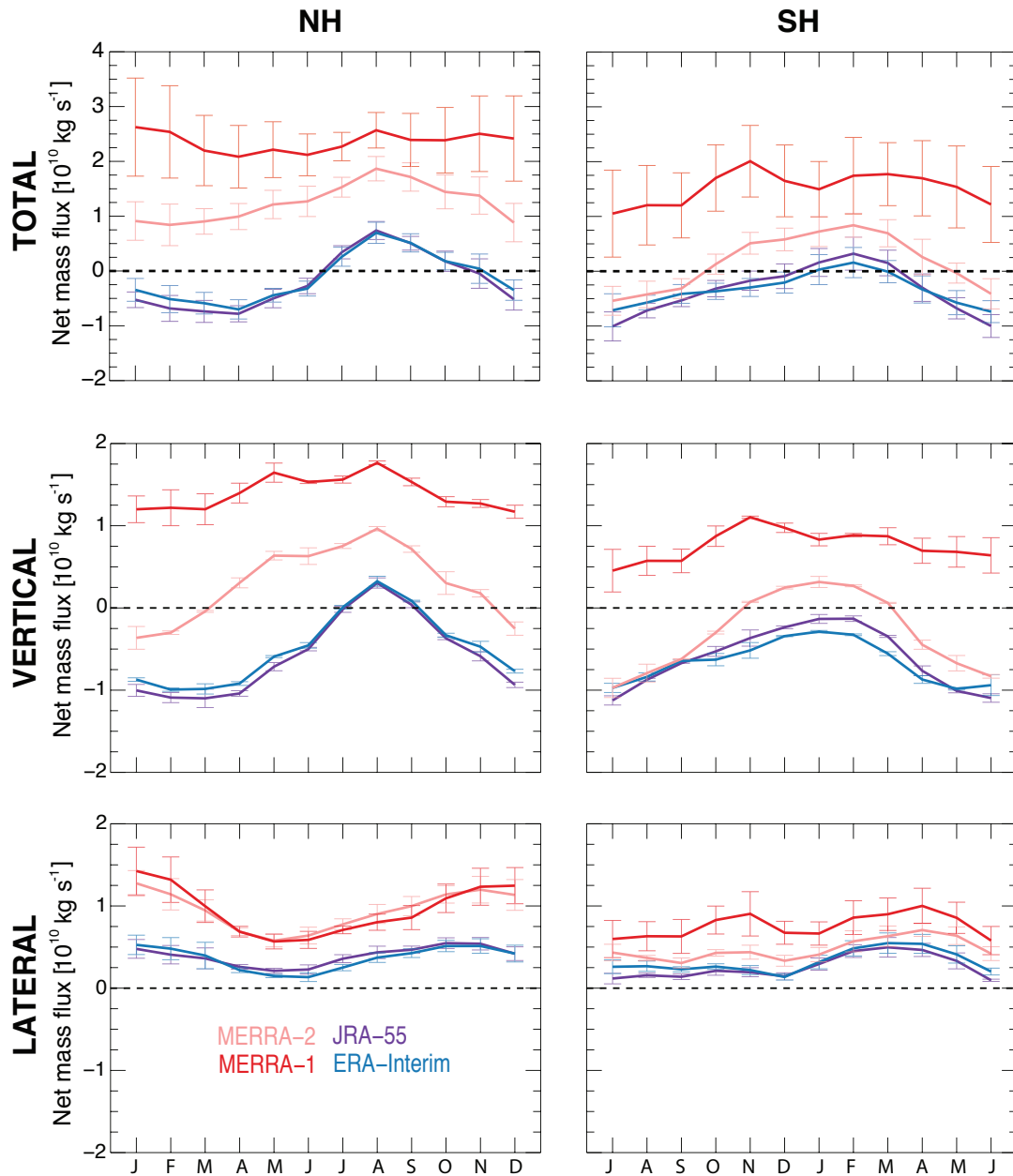


Figure 10: As in Figure 9, but for non-normalized net total STE (top row), net vertical STE (middle row), and net lateral STE (bottom row).

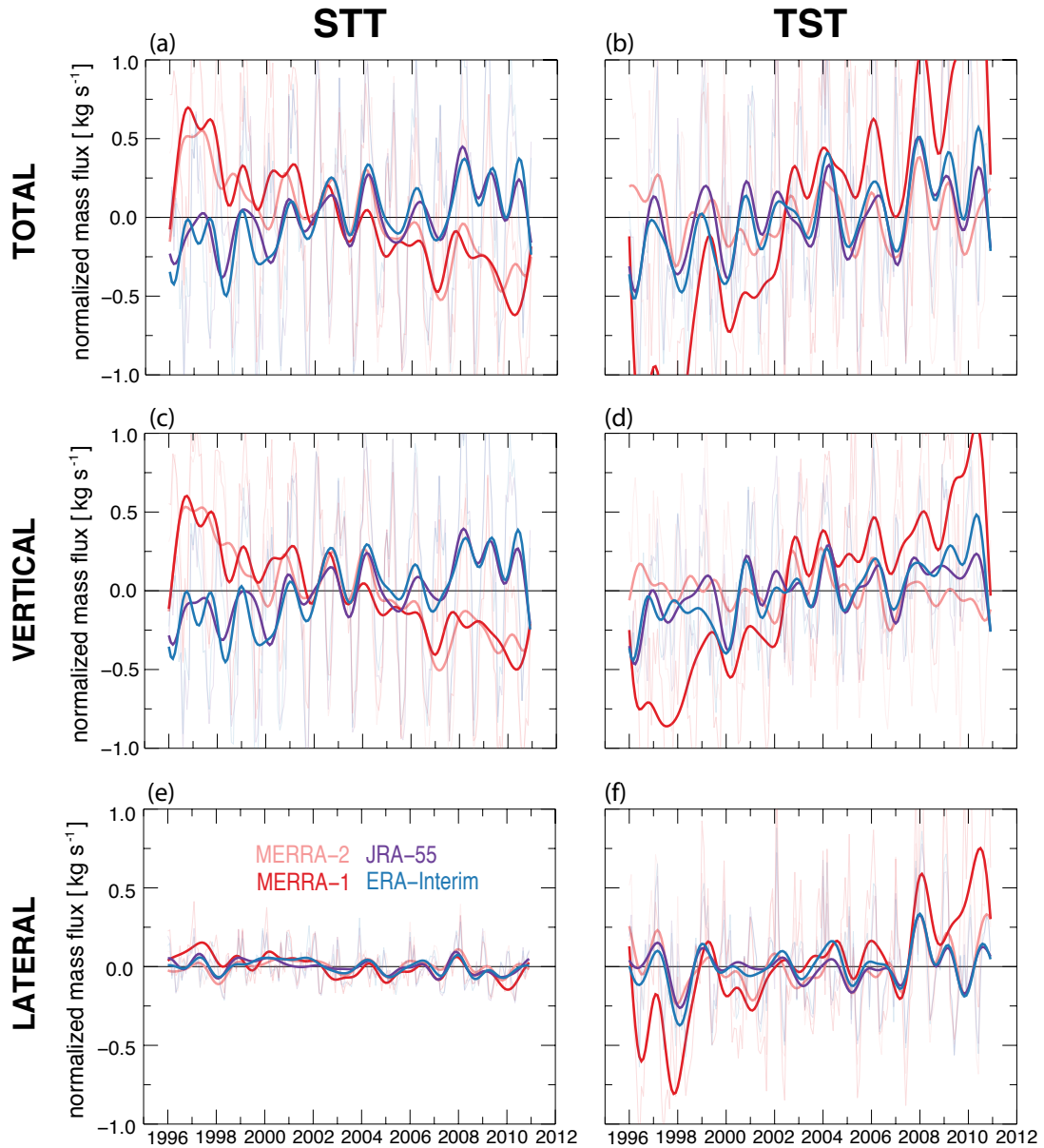


Figure 11: For each reanalysis, time series of globally integrated (top) total, (bottom) lateral, and (middle) vertical STT (left) and TST (right) mass fluxes that are normalized by the 15-year mean over the period (1996–2010). The thin lines represent the monthly mean mass fluxes, while the bold lines are the result of applying a low-pass filter to a Fourier transform of each time series (power at time scales ≤ 12 months is attenuated). STE from JRA-55 is shown by the purple lines, ERA-Interim by the blue lines, and MERRA-2 and MERRA-1 by the light and dark red lines, respectively.

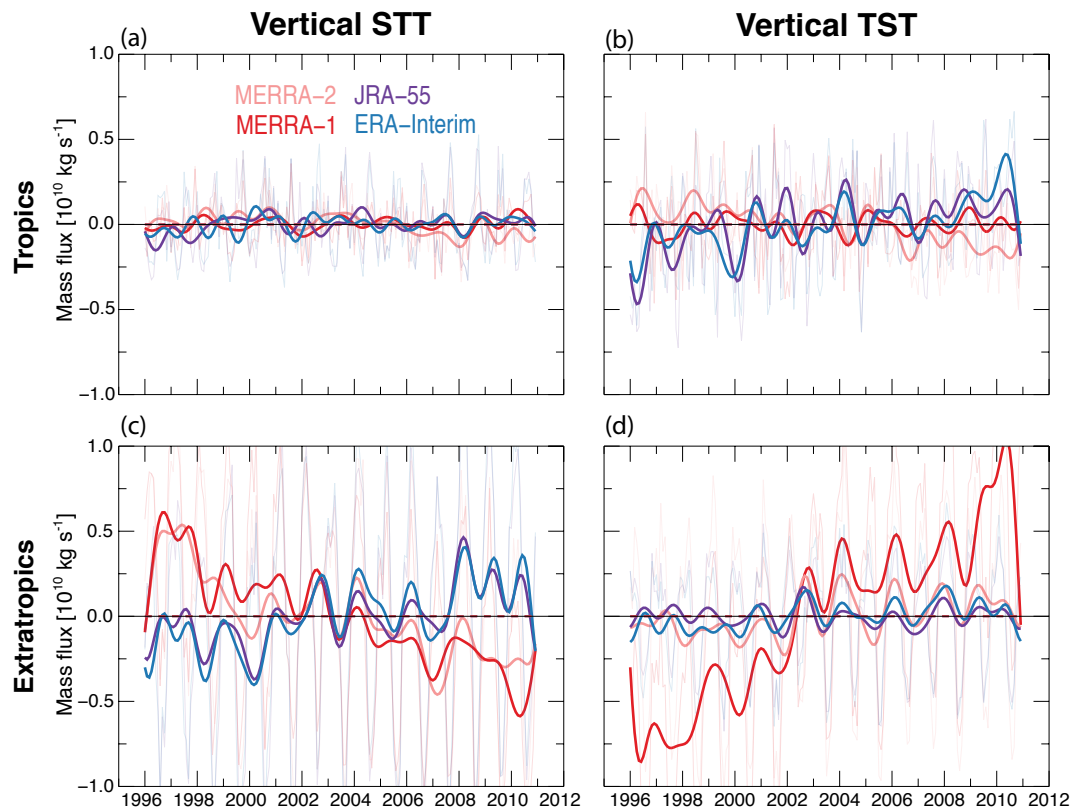


Figure 12: As in Fig. 11, but for vertical STE in the (top) tropics and (bottom) extratropics.

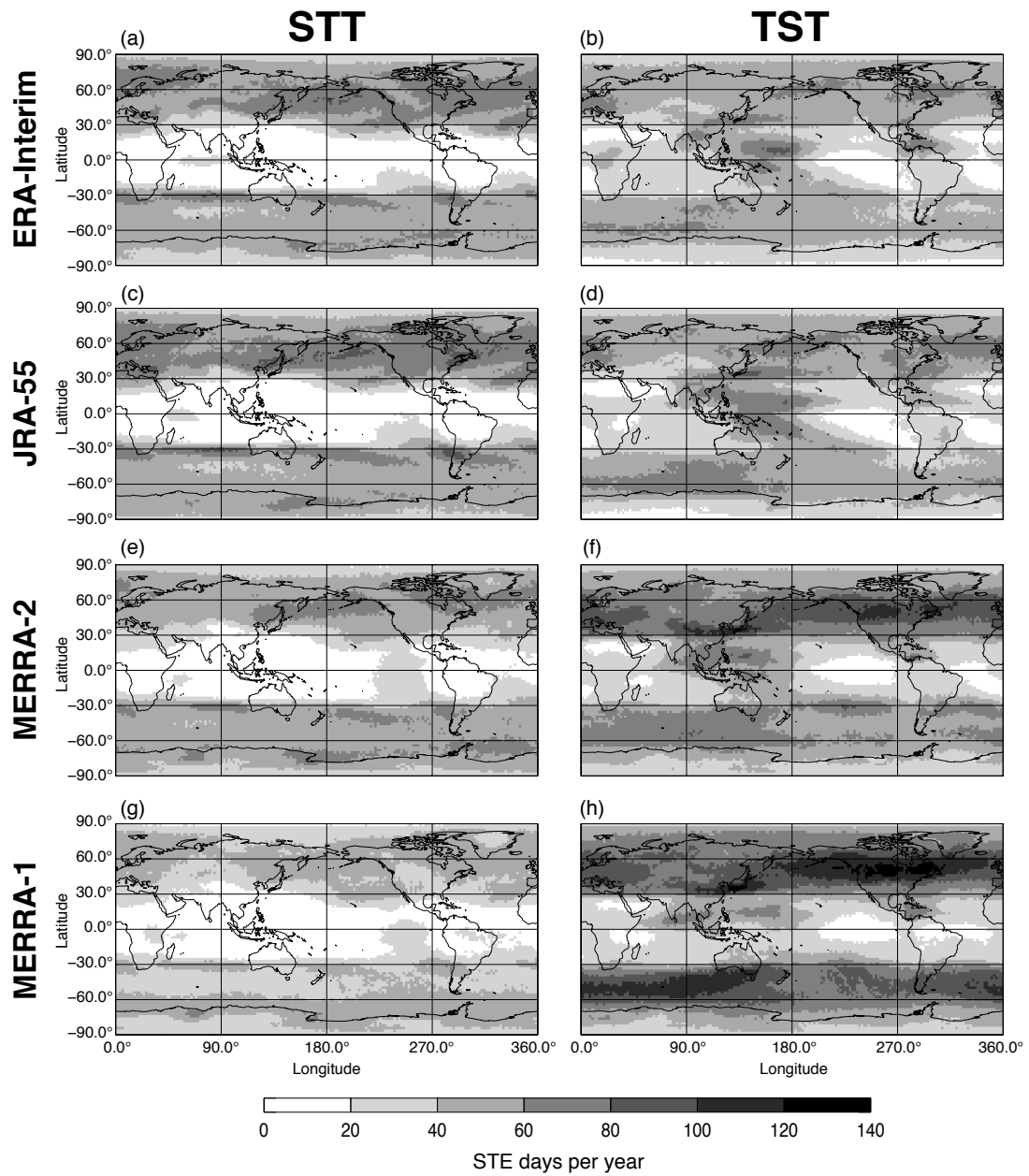


Figure 13: Global occurrence frequency distributions of (left) STT and (right) TST events for (a & b) ERA-Interim, (c & d) JRA-55, (e & f) MERRA-2, and (g & h) MERRA-1.

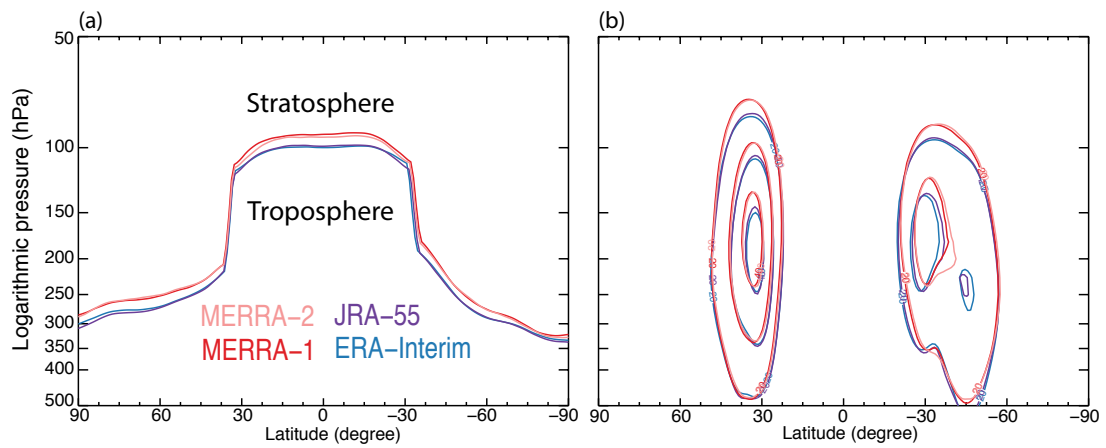


Figure 14: Monthly (November 2002) tropopause break-relative zonal means of (a) tropopause pressure (hPa) and (b) total horizontal wind (m s^{-1}) for each reanalysis. JRA-55 is shown by the purple lines, ERA-Interim by the blue lines, and MERRA-2 and MERRA-1 by the light and dark red lines, respectively.

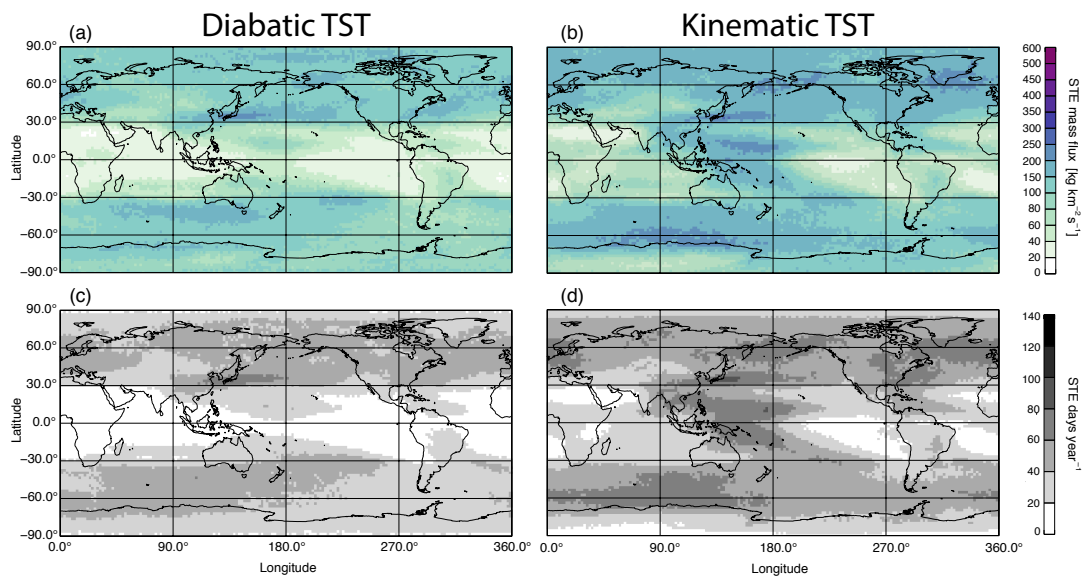


Figure 15: Geographic distributions of TST mass flux (top row) and occurrence (bottom row) using JRA-55 reanalysis diabatic (left; K s^{-1}) and kinematic (right; hPa s^{-1}) vertical velocity output over the 15-year period (1996–2010).